

# Continental contribution to the Marinoan cap carbonate of Tangará da Serra – MT, Brazil: further evidence from Sr-Nd-Pb isotope geochemistry

Nayra Michelly das Chagas Souza<sup>1</sup> , Jean Michel Lafon<sup>1</sup> , João Marinho Milhomem Neto<sup>1\*</sup> ,  
Joelson Lima Soares<sup>1</sup> 

## Abstract

On the southern edge of the Amazonian Craton, the Mirassol d'Oeste and Guia formations constitute the cap carbonate of the Araras Group. Petrography, X-ray diffraction, and quantification of terrigenous material allowed the identification of detrital grains (e.g., mica, quartz, and feldspar) in different proportions and diagenetic features. The sequential leaching of carbonates along a section of the upper portion of the Guia Formation yielded  $^{87}\text{Sr}/^{86}\text{Sr}$  ratios increasing from 0.7070 to 0.7077, which is considered the primary Sr isotopic signature of seawater. The increasing continental influx of dissolved Sr from freshwater accounts for the increase in  $^{87}\text{Sr}/^{86}\text{Sr}$  along the section. Such abrupt change toward more radiogenic values is also observed in carbonate layers soon after the Marinoan glaciation, elsewhere in the world. The same samples provided Nd- $T_{\text{DM}}$  model ages (1.84–2.54 Ga) comparable with those of the continental crust of the Paleoproterozoic provinces of the Amazonian Craton, which forms the basement of the Araras Group. The  $\epsilon_{\text{Nd}(635\text{Ma})}$  values between -4.7 and -11.1, probably indicate the presence of Nd from the suspended material transported by continental waters to the ocean where the carbonates precipitated. The random variations of Nd- $T_{\text{DM}}$  ages and  $\epsilon_{\text{Nd}}$  values suggest important and rapid variations in the continental contribution to the post-Marinoan oceans.

**KEYWORDS:** Amazonian Craton; Cap carbonate; Marinoan; Sr-Nd-Pb isotopes.

## INTRODUCTION

Important glacial episodes occurred on the planet during the Neoproterozoic due to pronounced paleoclimatic and paleogeographic changes. These glaciations are linked to the Snowball/Slushball Earth hypothesis, based on the partial/total freezing of the Earth's surface (Kirschvink 1992, Hoffman *et al.* 1998b, Hoffman and Schrag 2002). The most severe glacial episodes of this period were the Sturtian (717 to 659 Ma) and Marinoan (645 to 635 Ma) glaciations, immediately followed by greenhouse conditions in a still uncertain (low or high)  $\text{CO}_2$  atmospheric environment (Sansjofre *et al.* 2014, Hoffman *et al.* 2017, and the references therein) that promoted the deposition of post-glacial carbonate layers, which are called cap carbonates. Marine cap carbonates are described in different paleocontinents (see Hoffman *et al.* 2017 for compilation) and in South America (see Sial *et al.* 2016 for compilation). Marinoan cap carbonates are constituted by pinkish dolostones and gray limestones, which share typical features such as tube-like structures, giant stromatolites, megaripples, and crystal fans. Important  $^{87}\text{Sr}/^{86}\text{Sr}$  variations were observed worldwide

for the Marinoan cap carbonates from 0.7072 to > 0.7080 (Halverson *et al.* 2007, Bold *et al.* 2016, Verdel *et al.* 2018).

The global changes that provoked the formation of the Marinoan cap dolostones and their depositional environment are still widely discussed. Among the proposed models, the “plumeworld” (Shields 2005, Yang *et al.* 2017) and the alkaline weathering ones (Hoffman *et al.* 2017, Higgins and Schrag 2003) stand out. In the former model, the cap dolostone would have formed in a freshwater environment provided by the “plumeworld,” in which the ocean was well stratified between a saline and cold lower part and a fresh and hot upper part. In the latter model, the Marinoan limestones were formed in a mixed ocean (meltwater + saline water), which was highly acidified through the weathering of exposed carbonate platforms, generating a supersaturation of  $\text{CaCO}_3$  in the meltwater.

In Brazil, the record of Neoproterozoic post-glacial events is represented by the cap carbonates of the Bambuí and Vaza Barris/Miaba groups. The cap carbonate of the Bambuí group is found in the São Francisco craton and of the Vaza Barris/Miaba group in the Sergipano fold belt (Sial *et al.* 2010, Caxito *et al.* 2012, Alvarenga *et al.* 2014, Paula-Santos *et al.* 2017). The cap carbonate of the Araras Group crops out in the southwestern Amazon Craton, close to the Pimenta Bueno and Colorado grabens in Rondônia, and along the border of the Southern Amazon Craton with the intracratonic Cryogenian–Cambrian basin (Nogueira *et al.* 2019).

The available ages for the carbonate layer of the Araras Group (622–627 Ma, Pb-Pb whole rock; Babinski *et al.* 2006,

<sup>1</sup>Universidade Federal do Pará, Instituto de Geociências – Belém (PA), Brazil. E-mails: nayra.souza.m@gmail.com, lafonjm@ufpa.br, milhomem@ufpa.br, jlsoares@ufpa.br

\*Corresponding author.



Romero *et al.* 2013) agree with the U-Pb age of  $635.2 \pm 0.6$  and  $632.5 \pm 0.5$  Ma obtained in zircons from volcaniclastic levels in diamictites of the Doushantuo Formation, China, that provided an accurate radiometric reference for the Marinoan glaciation (Condon *et al.* 2005). Prave *et al.* (2016) also reported very accurate U-Pb ages of  $639.3 \pm 0.3$  and  $635.2 \pm 0.6$  Ma on zircon from ash beds from the Ghaub Formation in Namibia. The compilation of the available geochronological data bracketed the Marinoan glaciation between 649.9 and 634.7 Ma in different locations around the world (Hoffman *et al.* 2017).

The cap carbonate of the Araras Group overlies the Marinoan Puga glaciogenic diamictites and consists of the Mirassol d'Oeste and Guia formations (Nogueira *et al.* 2007; Soares and Nogueira 2008). The record of these formations is observed in the municipalities of Mirassol d'Oeste and Tangará da Serra, State of Mato Grosso, and the latter is the studied area in this study. The stratigraphy of the cap carbonate of the Tangará da Serra region was presented by Soares and Nogueira (2008) and updated by Soares *et al.* (2020). Variations in the  $^{87}\text{Sr}/^{86}\text{Sr}$  ratio of 0.7074–0.7080 and 0.7074–0.7078 were reported for the carbonate rocks of the Guia Formation by Nogueira *et al.* (2007) and Alvarenga *et al.* (2008), respectively, comparable with those found in cap carbonates elsewhere around the world. However, Romero *et al.* (2013) reported more restricted  $^{87}\text{Sr}/^{86}\text{Sr}$  ratios between 0.7071 and 0.7073 for the Guia Formation at Tangará da Serra.

The more radiogenic Sr isotopic signature from continental contribution compared with seawater has been used as a marker of the influence of glacial meltwaters on the oceans (Banner 2004). This continental signature is normally considered the effect of terrigenous minerals that are part of the mineralogical composition of carbonate rocks (mainly mica, feldspar, and clay minerals). Another possible contribution is the radiogenic Sr dissolved in continental waters, which may have been released to the oceans during the warming and incorporated by the carbonates at the time of its precipitation.

In addition to Sr, the Nd isotopic signature can be used as complementary evidence to distinguish continental and open ocean sources and their variation in the carbonates can depict a continental contribution that modified the chemical composition of seawater, as it occurs immediately after the great glaciations (Banner 2004, Caxito *et al.* 2012 and references therein). A Nd isotopic study of carbonates from the Araras Group and of other sedimentary sequences of the Paraguay Belt evidenced a continental contribution from Paleoproterozoic sources (Dantas *et al.* 2009).

This study aimed to determine the Nd-Sr isotopic signatures of Ediacaran carbonate rocks from the southern Amazonian Craton soon after the Marinoan glaciation and evaluate the effects of the continental contribution linked to the post-glacial melting, during carbonate precipitation. For this purpose, the variations in the  $^{87}\text{Sr}/^{86}\text{Sr}$  and  $^{143}\text{Nd}/^{144}\text{Nd}$  ratios along a section of the Guia Formation were determined and related to continental influence. On a global scale, the study is a further contribution to the elaboration of the Ediacaran seawater Sr evolution curve. In addition, further Pb isotope analyses were performed to improve the precision on the age of  $622 \pm 33$

Ma, which was previously determined for the carbonates of the Guia Formation by Romero *et al.* (2013).

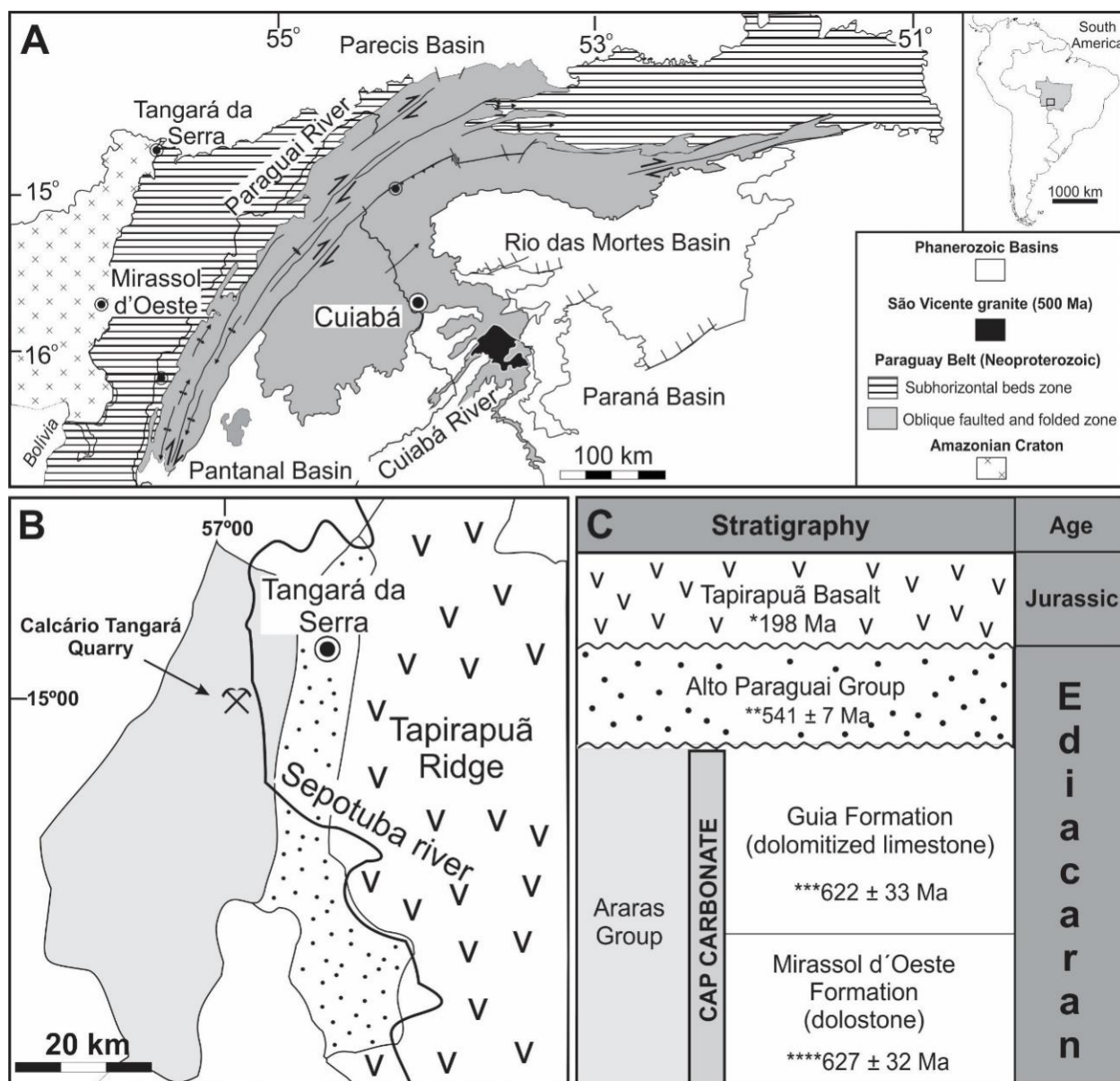
## GEOLOGICAL CONTEXT

The study area is located at the southern border of the Amazonian Craton, the largest cratonic area in South America, with the Paraguay belt, which is an extensive Neoproterozoic orogenic belt (Fig. 1). The Neoproterozoic carbonate rocks distributed in several areas of the State of Mato Grosso have been included in the Araras Group, as defined by Almeida and Hasui (1984). The Araras Group consists of a predominantly carbonatic succession with a thickness greater than 1,200 m, which lies above the glacial diamictites of the Puga Formation, and is inconsistently covered by the siliciclastic deposits of the Alto Paraguay Group (Nogueira and Riccomini 2006, Bandeira *et al.* 2007). It is divided into four formations, from bottom to top (Nogueira and Riccomini 2006):

- I. Mirassol d'Oeste Formation, formed by dolomudstone and pink dolomudstone with peloids, with a thickness of up to 20 m in the sector of Mirassol d'Oeste, where the succession is more complete (Nogueira *et al.* 2019);
- II. Guia Formation, which consists of a succession of bituminous calcareous mudstones, shales, and cementstones with fans of calcite crystals, with a total thickness of 200 m;
- III. Serra do Quilombo Formation, consisting of breccias and dolomites with a total thickness of 100 m;
- IV. Nobres Formation, about 200 m thick, formed by dolomite, sandy dolomite, microbialites, flint, and sandstone (Rudnitzki *et al.* 2016).

Facies analysis suggests that the depositional environment evolved from a moderately deep to shallow carbonate platform, influenced by  $\text{CaCO}_3$  supersaturation, seismic, and storm events (Mirassol d'Oeste, Guia, and Serra do Quilombo formations) to a carbonate shallow platform (Nobres Formation), influenced by waves and characterized by environments of sabkha and tidal plain (Nogueira and Riccomini 2006).

In the Tangará da Serra area, the Mirassol d'Oeste Formation is formed by fine to coarse-grained pink-colored dolograins, interpreted as the “dolomitic layer,” macropeloids associated with laminations with truncations, peloids, and massive siltstone and laminates interspersed with fine crystalline limestones with megaripples and tube-like structures associated with giant domal stromatolites (Santos *et al.* 2021). The abrupt contact of the cap carbonate with structures of soft-sediment deformation due to rapid loading of the carbonate package over the unconsolidated diamictite (Nogueira *et al.* 2007) indicates a change from icehouse to greenhouse conditions. The Guia Formation consists of fine crystalline limestones, bituminous shales, and detrital grains. It also presents cementstones with fans of calcite crystals (pseudomorphs of aragonite) nucleated at the base of irregular to planar thin cement crusts. This Formation is associated with a deep platform environment supersaturated in  $\text{CaCO}_3$ , and its base probably represents a diachronic (transgressive) surface (Nogueira *et al.* 2007, Sansjofre *et al.* 2014).



Source: adapted from Soares and Nogueira (2008).

**Figure 1.** Studied area location. (A) Geotectonic context. (B) Simplified geological map of the Tangará da Serra region, with the Calcário Tangará Quarry. (C) Stratigraphic chart of lithostratigraphic units that occurred in the Tangará da Serra region. Ages based on \*Marzoli *et al.* (1999)  $^{40}\text{Ar}/^{39}\text{Ar}$  method, \*\*Bandeira *et al.* (2012)-detrital zircon U-Pb maximum depositional age, \*\*\*Romero *et al.* (2013)-carbonate Pb-Pb dating, and \*\*\*\*Babinski *et al.* (2006)-carbonate Pb-Pb dating.

Carbon and oxygen isotopic data,  $^{87}\text{Sr}/^{86}\text{Sr}$  signatures, and Pb-Pb ages were published for the cap carbonate of the Araras Group. In the Mirassol d'Oeste area, strongly negative  $\delta^{13}\text{C}$  values were found for the Mirassol d'Oeste Formation (-10.5‰ to -4.1‰) and for the Guia Formation (-5.4‰ to -2.7‰) with  $\delta^{18}\text{O}$  values of -10.0‰ to -2.0‰ and -6.0‰ to -1.3‰, respectively (Alvarenga *et al.* 2008). Similar results were obtained for the base of the Guia Formation in the sector of Nobres, in the northern portion of the Paraguay Belt, with  $\delta^{13}\text{C}$  values between -4.5‰ and -3.5‰ (Paula-Santos *et al.* 2010). In the Tangará da Serra area, the  $\delta^{13}\text{C}$  values of the cap carbonate range from -7.0‰ to -4.0‰ (Soares and Nogueira 2008), and the  $\delta^{18}\text{O}$  values between -8.1‰ and -1.4‰ (unpublished data from Soares 2012). According to Jacobsen and Kaufman (1999), a value of  $\delta^{18}\text{O} > -10\text{‰}$  indicates that  $\delta^{13}\text{C}$  values record the primary marine value, as it happens in the cap carbonate of the Araras Group. The similarity of the  $\delta^{13}\text{C}$  and  $\delta^{18}\text{O}$  data between the cap

carbonate of the Mirassol d'Oeste and Tangará da Serra areas reinforced their stratigraphic correlation (Nogueira *et al.* 2019). The  $\delta^{13}\text{C}$  curve of the Araras Group shows the same pattern as other Marinoan cap carbonates elsewhere in the world, such as in northwestern Canada, Namibia, China, Oman, and Australia (Nogueira *et al.* 2019 and the references therein).

The  $^{87}\text{Sr}/^{86}\text{Sr}$  ratios between 0.7071 and 0.7073 of carbonates at the base of the Guia Formation in the Tangará da Serra area were considered to depict the primary signature of Sr from ocean waters at the beginning of Ediacaran in the south of the Amazonian Craton (Romero *et al.* 2013). They are among the lowest values for Marinoan cap carbonates, along with those from the Hayhook Formation in Canada (Halverson *et al.* 2007). These low and homogeneous  $^{87}\text{Sr}/^{86}\text{Sr}$  values contrast with the higher and more variable ones (0.7074–0.7080) previously obtained for the Guia Formation (Nogueira *et al.* 2007; Alvarenga *et al.* 2008). Such a difference raised the question

of a possible contribution of terrestrial material, which could modify the primary Sr signature of carbonates. This assumption is justified by the different procedures used for the dissolution of carbonates. Nogueira *et al.* (2007) and Alvarenga *et al.* (2008) used a strong acid (hydrochloric acid), which may have partially removed Sr from siliciclastic minerals. In turn, Romero *et al.* (2013) used a weak and diluted acid (acetic acid) in the sequential dissolution of carbonates that minimizes the leaching of Sr from siliciclastic components (Bailey *et al.* 2000).

Pb-Pb dating of cap carbonates of the Araras Group provided early Ediacaran ages for carbonate deposition that confirmed their relationships with the Marinoan Glaciation ( $\approx 635$  Ma) at the Cryogenian–Ediacaran transition. Carbonates from the Terconi Mine in the Mirassol d'Oeste region yielded an age of  $627 \pm 22$  Ma (Babinski *et al.* 2006). In the region of Tangará da Serra, Romero *et al.* (2013) obtained an age of  $622 \pm 33$  Ma for the carbonates of the Guia Formation.

## SAMPLING AND ANALYTICAL PROCEDURES

The samples come from the upper portion of the Guia Formation, at the Calcário Tangará Quarry, in Tangará da Serra, and they have been collected during the field campaign carried out by Romero *et al.* (2013). The section height is 65 m, and the samples are from the upper portion of the section between 45 and 65 m, above those between 30 and 42 m used by Romero *et al.* (2013). Eleven samples were selected for Sr-Nd analyses, of which the Sr isotopic ratio of the most basal had already been determined by Romero *et al.* (2013) (Fig. 2).

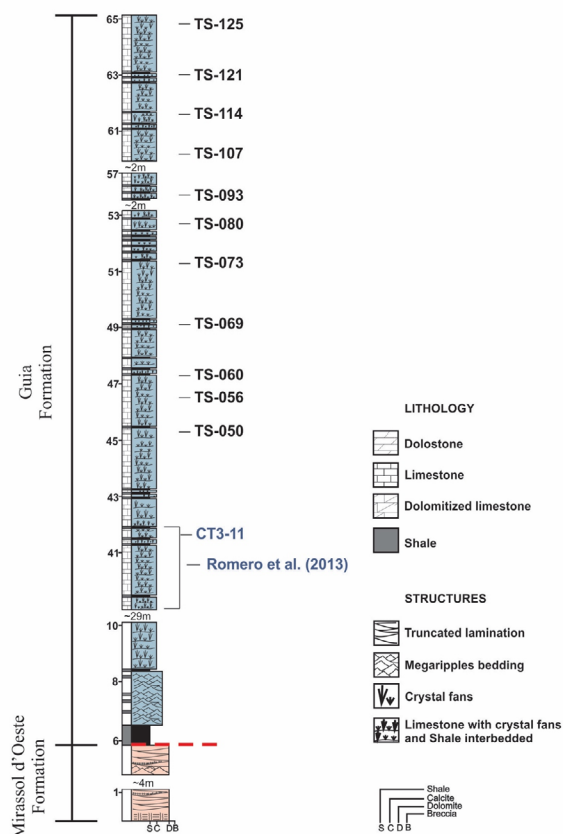


**Figure 2.** Stratigraphic section of the Guia Formation at the Calcário Tangará Quarry with the location of the samples along the section.

The samples were selected for the petrographic description of thin sections, quantification of the siliciclastic material, mineral identification of the siliciclastic phase, and isotopic and geochronological analyses of Sr, Nd, and Pb (the latter, only in three samples). All analyses were performed in laboratories of the Instituto de Geociências at the Universidade Federal do Pará, Belém, Brazil.

The petrographic description was performed at the Petrography Laboratory of the Research Group on Sedimentary Basin Analysis of the Amazon — GSED using a LEICA DM 2700P petrographic microscope equipped with a digital camera. The identification of the main depositional and diagenetic constituents and the classification of microfacies followed the proposals of Wright (1999) and Flügel (2004). For petrographic classification, Dunham's (1962) proposal was adopted. Tucker's classification (1992) was used to distinguish calcite crystals according to their size. In addition, Alizarin-S and potassium ferrocyanide were used to assist in differentiating between calcite and dolomite.

The quantification of the terrigenous material was made by weight difference after acid dissolution with 2N HCl of about 5 g of the sample until a total elimination of the carbonate phase. The siliciclastic residue was analyzed by X-ray diffraction to identify the mineralogical composition at the Mineral Characterization Laboratory (LCM) with an Empyrean PANanalytical spectrometer, with Goniometer QQ and ceramic X-ray tube of Cobalt anode ( $K\alpha_1 = 1, 78,901$  Å). Data acquisition was done with the X'Pert Data Collector software, version 5.1, and the data reduction with the X'Pert HighScore Plus software, version 3, also from PANanalytical. The analysis parameters and conditions are described in detail by Paz *et al.* (2018).

Isotopic abundances of Sr, Nd, Sm, and Pb were determined at the Isotope Geology Laboratory (Pará-Iso). Nd, Sm, and Pb isotopic analyses were carried out on a Thermo-Finnigan Neptune multi-collector inductively coupled plasma mass spectrometer (MC-ICP-MS). Sr isotopic analyses were performed on a Finnigan MAT 262 thermo-ionization mass spectrometer (TIMS), except for sample TS-093 which was analyzed by MC-ICP-MS.

The sequential dissolution procedure to extract Sr from the carbonate fraction described by Bailey *et al.* (2000) was used. Around 200 mg of the sample was dissolved with 150 mL of 20% acetic acid diluted in 2 mL of milli-Q® H<sub>2</sub>O until the reaction was over. After centrifugation, the supernatant was removed for further analysis. This leaching cycle was repeated successively until the complete dissolution of the carbonate phase, leaving only a siliciclastic residue. The extraction and purification of Sr from the supernatant of each leaching step were carried out by ion exchange chromatography with Eichrom® Sr 50–100 µm resin. For the isotopic analyses by TIMS, the Sr concentrate was mixed with a tantalum activator solution and deposited on a tungsten filament. For isotopic analysis by MC-ICP-MS, the Sr concentrate of sample TS-093 was conditioned in 3% HNO<sub>3</sub>. The isobaric interferences of Kr (krypton) from the argon carrier gas on the <sup>84</sup>Sr and <sup>86</sup>Sr masses were corrected by monitoring the <sup>82</sup>Kr and <sup>83</sup>Kr masses and assuming their

natural isotopic abundances. In both mass spectrometers, Sr isotopic ratios were corrected internally for mass discrimination using a value of 0.1194 for the  $^{86}\text{Sr}/^{88}\text{Sr}$  ratio.

For the determination of the Nd isotopic composition and Sm and Nd concentrations, about 500 mg of sprayed sample was dissolved together with 100 mg of mixed  $^{149}\text{Sm}$ - $^{150}\text{Nd}$  tracer with 2N HCl\*\*\* for 24 h. The sample was evaporated after ultrasonic cleaning. This procedure was repeated until the total dissolution of the carbonate phase. Finally, the residue was dissolved in 2N HCl\*\*\* and the solution was centrifuged to remove the supernatant and then evaporated. The extraction of Sm and Nd was carried out by ion exchange chromatography in two stages using a Biorad Dowex AG50W-X8 resin and Eichrom® 50–100  $\mu\text{m}$  Ln resin, according to the procedure described in Barreto *et al.* (2014). The isotopic compositions of Nd and Sm were determined by MC-ICP-MS. The Nd isotopic ratios were normalized using a  $^{146}\text{Nd}/^{144}\text{Nd}$  ratio of 0.7219 and the  $^{147}\text{Sm}/^{144}\text{Nd}$  ratio allowed the correction of Sm interference. The  $^{149}\text{Sm}/^{147}\text{Sm}$ ,  $^{152}\text{Sm}/^{147}\text{Sm}$ , and  $^{155}\text{Gd}/^{147}\text{Sm}$  ratios were used, respectively, to calculate the isotopic dilution and instrumental isotopic fractionation and to correct the gadolinium interference.

For the Pb isotopic analyses, about 500 mg of sample was dissolved by repeated addition of 48% HF\*\* and concentrated  $\text{HNO}_3$ \*\*. The Pb was extracted by ion exchange chromatography with Eichrom® 50–100  $\mu\text{m}$  Sr resin and dissolved in a solution of  $\text{HNO}_3$  3% + Tl (thallium) 50 ppb for isotopic

analysis by MC-ICP-MS. Thallium was used to correct the Pb isotopic ratios from instrumental isotopic fractionation during the analysis (Platzner *et al.* 2001).

## RESULTS

### Microfacies

Two microfacies were identified: mudstone and cementstone. The mudstone is formed by microcrystalline calcite, locally interspersed with fine laminations of terrigenous grains (Fig. 3A). Peloids of varying sizes also occur, with microcrystalline calcite composition and without internal structures. Cementstone is characterized by arborescent calcite crystal fans (aragonite pseudomorphs) and a millimeter-scale calcite crust. Rhombohedral and anhedral crystals of ferrous dolomite (pale olive-green dolomite) occur widely in the microcrystalline matrix and the calcite fans.

The two microfacies appear interspersed and form irregular laminations (Fig. 3B). Crystal fans are abundant in the cementstone microfacies and occur in all thin sections in the acicular form commonly associated with the calcite crust or isolated (Fig. 3C). Microcrystalline calcite occurs interspersed with lamination of terrigenous grains (quartz, feldspar, and a few micas) in the mudstone microfacies (Fig. 3D). These features are similar to those previously described for carbonates of the same formation (Romero *et al.* 2013).

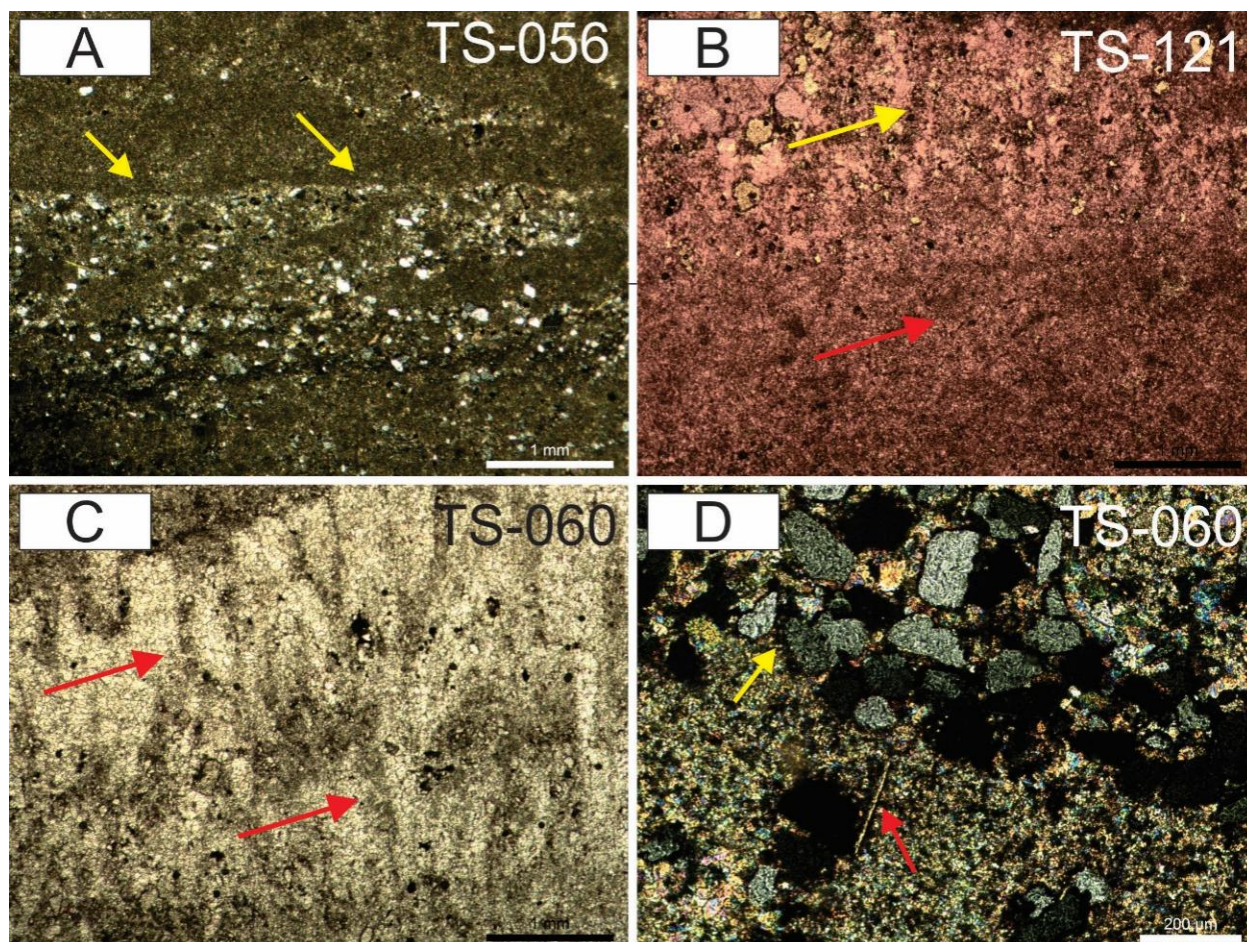


**Figure 3.** Characteristics of the carbonates from the Guia Formation at the Calcário Tangará Quarry. (A) Terrigenous grains interspersed with microcrystalline calcite, indicated by yellow arrows. (B) Microfacies mudstone (red arrow) and cementstone (yellow arrow). (C) Microfacies cementstone, characterized by the crystal fans of calcite (red arrows). (D) Terrigenous grains: quartz (yellow arrow) and mica (red arrow).

## Diagenetic features

The diagenetic features include neomorphism in microcrystalline primary calcite and replacement in aragonite fans with sparry calcite (Fig. 4A) and chemical compaction, which occurs as stylolites and dissolution seams in all layers (Fig. 4B), accompanied by terrigenous grains and iron oxide (Fig. 4C). Microfractures filled with microsparry calcite are also found in carbonates (Fig. 4D).

The features suggest that the diagenetic processes occurred mainly during burial. They did not show a gradation along the profile, and all samples were similarly affected by diagenesis. Neomorphism was the first diagenetic event that mainly affected carbonate mud and aragonite crystals. This process may have occurred near the sediment–water interface or a few meters deep (Tucker 1992). Features such as fracturing, dolomitization, and chemical compaction, observed in the limestones, can indicate deep burial (Tucker 1992, Flügel 2004).

## Siliciclastic component: identification and quantification

Microcrystalline calcite, peloids, acicular crystals, and crusts of microsparry calcite and iron oxide are common to all samples but vary in abundance. Terrigenous grains are quartz, feldspar, and mica (Fig. 5). Microcrystalline and microsparry calcites are predominantly ferrous and locally

of magnesian composition (identified by their reddish color). Quartz is the most abundant terrigenous mineral and occurs as angular and subangular grains, sometimes forming aggregates between calcite fans or discontinuous laminations. Feldspars occur as angular grains, and most of them preserve their twinning. Micas are rare, commonly small, and display a lamellar shape. These characteristics make it difficult to distinguish the type of mica that occurs in these rocks.

For the quantification and identification of the terrigenous material in the carbonate samples, X-ray diffraction was carried out on the residue to ensure that the complete dissolution of the carbonatic phase was achieved and to identify the mineralogical composition of the siliciclastic component. This procedure was performed on all samples, and the results are shown in Table 1 and Fig. 6.

In the 11 samples, quartz is the dominant peak, followed by K-feldspar and less mica. The peak corresponding to pyrite appears in all samples with varying intensity. The composition of the siliciclastic material is quite similar in all samples as illustrated in Fig. 6 where the diffractograms are presented in groups and individually. The sample TS-107 showed no difference from the other samples, despite having a much higher proportion of terrigenous grains ( $\approx 20\%$ ) compared with the other samples ( $\approx 6\text{--}14\%$ ). In the thin section, this sample was similar to the other ones.

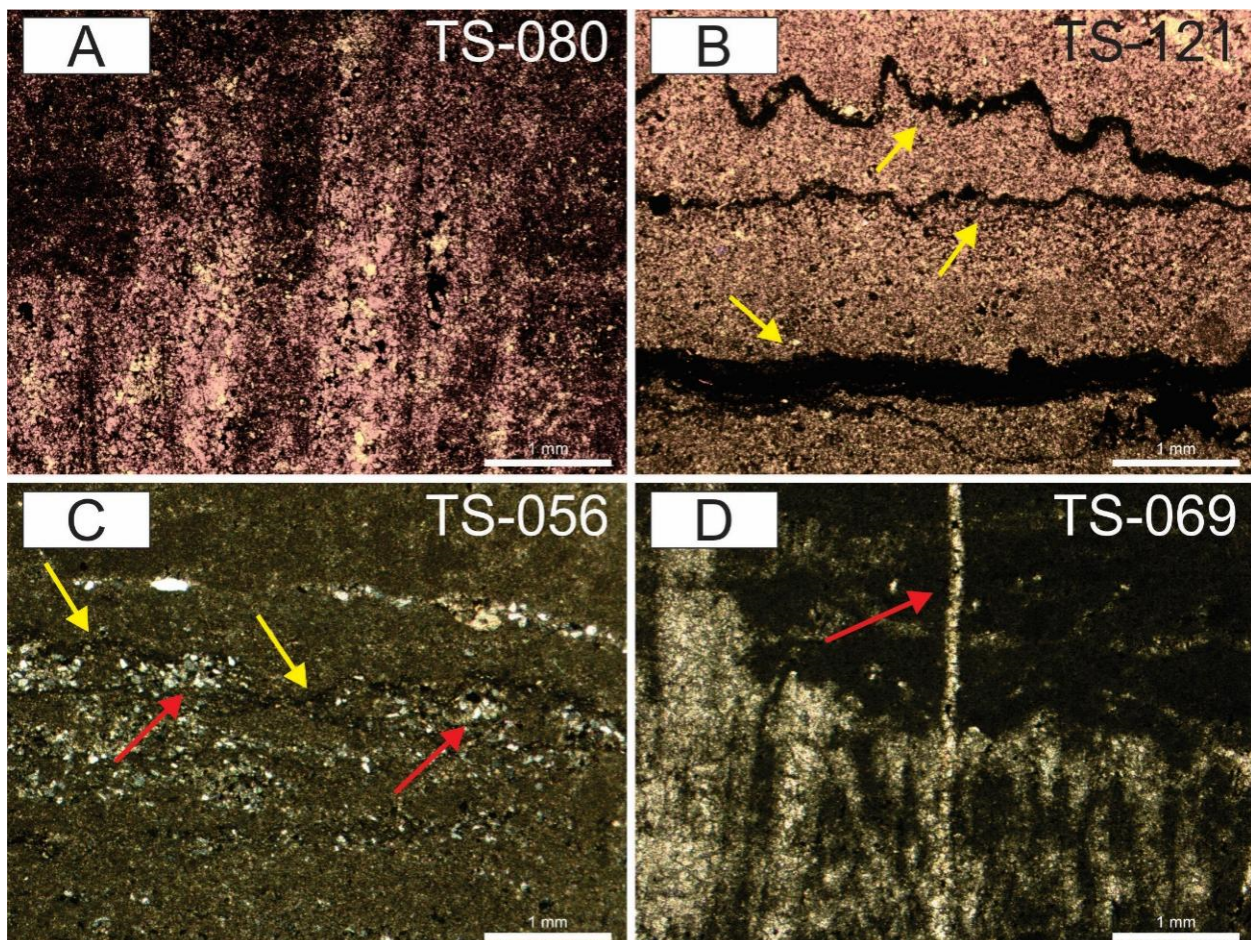


**Figure 4.** Diagenetic features of the carbonates of the Guia Formation: (A) replacement of aragonite by sparry calcite in the crystal fans, indicated by different colors after dyeing; (B) stylolite and dissolution seams (yellow arrows); (C) stylolite (yellow arrows) accompanied by terrigenous grains (red arrows); (D) microfractures filled by microsparry calcite (red arrow).

## Pb-Pb geochronology

Pb-Pb isotopic analyses were performed on the following three samples: TS-080, TS-107, and TS-121, after total dissolution of the carbonate phase and siliciclastic material (Table 2). The samples did not allow a greater spread of the analytical points when plotted in the  $^{207}\text{Pb}/^{204}\text{Pb}$  vs.  $^{206}\text{Pb}/^{204}\text{Pb}$  diagram together with the samples by Romero *et al.* (2013) (Fig. 7). The analytical points of the samples analyzed in this study are close to those with less radiogenic composition and the isochron calculation provided an age of  $622 \pm 30$  Ma like that determined by Romero *et al.* (2013), with slightly better accuracy ( $\pm 30$  Ma instead of  $\pm 33$  Ma).

## Sr isotopic results

For each sample, up to nine aliquots resulting from sequential leaching were analyzed. In some aliquots, the isotopic composition was not determined due to the very low intensity of the Sr analytical signal.

The  $^{87}\text{Sr}/^{86}\text{Sr}$  ratios showed large variations from one aliquot to another in the same sample (Table 3) but without any clear upward or downward trend. In samples TS-125, TS-107, TS-080, TS-069, and TS-056, the last aliquot (L8 or L9) is much more radiogenic than those of the previous stages of leaching. For the samples that provided nine aliquots, values range from 0.7180 (sample TS-080) to 0.7373 (sample TS-107). For most of the samples, the first aliquots (L1 and L2) yield  $^{87}\text{Sr}/^{86}\text{Sr}$  values that are slightly more radiogenic than

the following ones, ranging from 0.70718 (sample TS-050) to 0.70791 (sample TS-121). The lowest  $^{87}\text{Sr}/^{86}\text{Sr}$  values (0.70705–0.70708) were obtained for samples TS-050 and TS-056, which are the lower samples from the studied part of the section. The samples TS-114, TS-093, and TS-050 showed the smallest internal variations in the  $^{87}\text{Sr}/^{86}\text{Sr}$  ratio. For each sample, a weighted average of the overlapping values at a  $2\sigma$  level of the lowest  $^{87}\text{Sr}/^{86}\text{Sr}$  ratios was calculated.

**Table 1.** Quantification of the abundance of terrigenous grains.

Sample	Initial weight (mg)	Final weight (mg)	Carbonatic phase (wt%)	Terrigenous grains (wt%)
TS-125	5,002.0	488.8	91.2	9.8
TS-121	4,999.3	666.7	86.7	13.3
TS-114	5,006.3	484.5	91.3	9.7
TS-107	5,000.0	988.9	80.2	19.8
TS-093	5,002.6	545.5	89.1	10.9
TS-080	4,999.9	463.3	90.7	9.3
TS-073	5,002.2	552.0	89.0	11.0
TS-069	4,999.4	559.9	88.8	11.2
TS-060	4,999.5	468.3	90.6	9.4
TS-056	4,999.7	484.3	90.3	9.7
TS-050	5,005.6	295.6	94.1	5.9
CT3-11	5,014.3	501.3	90.0	10.0

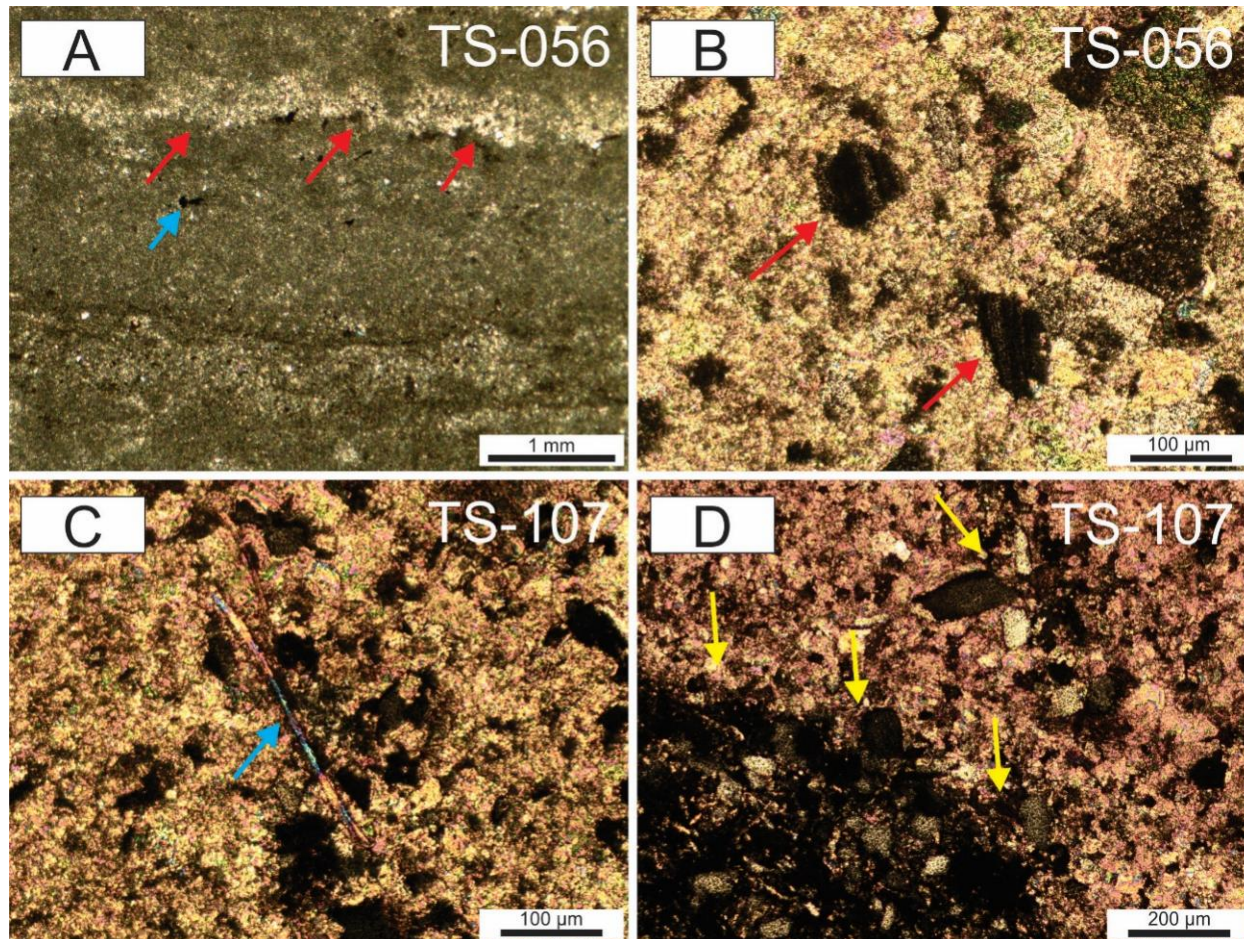


**Figure 5.** Mineralogical composition of carbonates: (A) crust of microsparry calcite (red arrows) and iron oxide (blue arrows); (B) K-feldspar crystals with corroded edges; (C) mica with lamellar structure (blue arrow); (D) quartz grains with different shapes and aggregates (yellow arrows).

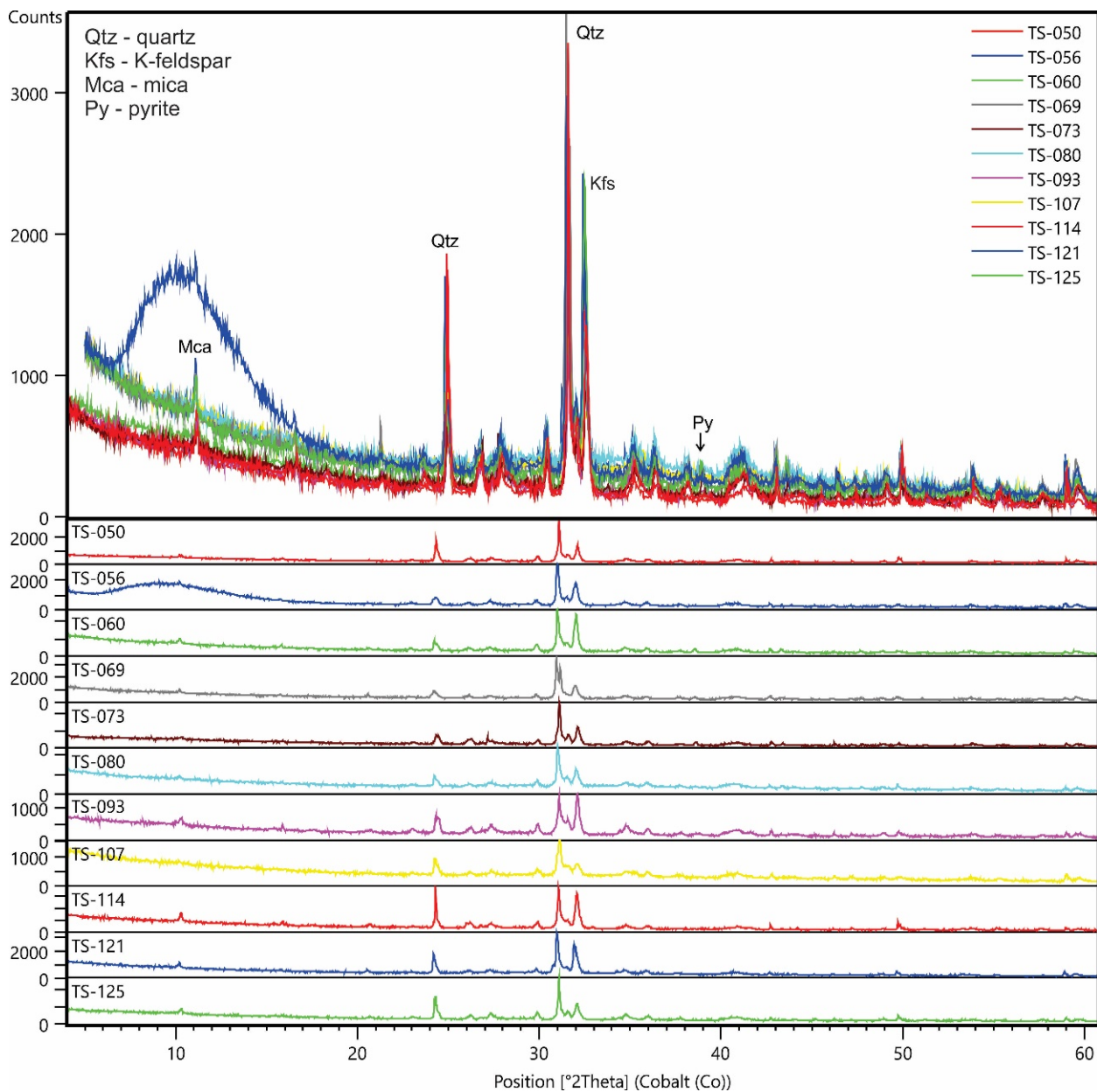


**Figure 6.** X-ray diffractograms for the 11 analyzed samples grouped and individual (X-ray diffraction was not performed on the CT3-11 sample).

**Table 2.** Pb isotopic composition determined by ICP-MS for the three carbonate samples (total carbonate dissolution).

Amostra	$^{206}\text{Pb}/^{204}\text{Pb}$	2s	$^{207}\text{Pb}/^{204}\text{Pb}$	2s	$^{208}\text{Pb}/^{204}\text{Pb}$	2s
TS-080	21.037	0.008	15.861	0.006	38.586	0.015
TS-107	18.899	0.003	15.723	0.003	38.407	0.010
TS-121	19.390	0.006	15.745	0.005	38.499	0.015

In two samples (TS-107 and TS-093), the aliquots with lower  $^{87}\text{Sr}/^{86}\text{Sr}$  ratios do not overlap and the aliquot that provided the lowest  $^{87}\text{Sr}/^{86}\text{Sr}$  ratio (L8 and L7, respectively) was used for interpretation.

### Nd isotopic results

Nd isotopic analyses were performed on the 11 samples analyzed for Sr, plus the sample CT3-11 previously analyzed for Sr isotopes by Romero *et al.* (2013). The Nd results, including  $\epsilon_{\text{Nd}}$  and model ages ( $\text{Nd-T}_{\text{DM}}$ ), are shown in Table 4. The  $\epsilon_{\text{Nd}}$  values were calculated at 635 Ma, corresponding to the age of termination of the Marinoan Glaciation.

The  $^{143}\text{Nd}/^{144}\text{Nd}$  values vary from 0.511838 to 0.512167, and the  $\epsilon_{\text{Nd}}$  values vary from -11.1 to -4.7. The calculation of  $\text{Nd-T}_{\text{DM}}$  ages using the model of DePaolo (1981) provided values between 1.85 and 2.54 Ga. In a  $^{143}\text{Nd}/^{144}\text{Nd}$  vs.  $^{147}\text{Sm}/^{144}\text{Nd}$  diagram, the analytical points did not fit a straight line and it was not possible to calculate an isochronic age.

### DISCUSSION

The strontium isotopic data of marine carbonates, when the signature is considered primary, reflect the variation of the  $^{87}\text{Sr}/^{86}\text{Sr}$  ratio of seawater from which the carbonate

precipitated. For Neodymium, the isotopic ratios can reveal information about the provenance and tectonic evolution of the sedimentary basin and its interior (Halverson *et al.* 2010). Both data complement each other in the attempt to identify possible variations in the sources involved in oceanic waters that gave rise to Marinoan cap carbonates. To assist in these interpretations, petrography, X-ray diffraction, and the quantification of siliciclastic material of

the limestones of the Guia Formation were used to identify the mineralogical assembly and assess the influence of terrigenous components. In addition, the Pb isotopic data aimed to strengthen the determination of the age of formation of the cap carbonate.

Through the petrographic study, it was possible to identify diagenetic characteristics, such as neomorphism, chemical compaction, and dolomitization, which occurred to the same degree in all samples, in addition to a significant amount of disseminated terrigenous material, as previously described (Soares and Nogueira 2008, Romero *et al.* 2013). Despite the diagenesis, typical features have still been preserved, such as the lamination and the aragonite fans that have been replaced by calcite. Terrigenous grains occur clustered, usually along dissolution seams, in most of the samples.

X-ray diffraction revealed quartz, potassium feldspar, and mica, in addition to iron oxide/hydroxide and pyrite as the terrigenous. This mineralogical association is the typical one for the terrigenous suspended material transported from continental areas into the platform environment where the Guia Formation is deposited. The same association was reported in samples from Romero *et al.* (2013). The low peaks of pyrite show that it is present in a small amount, which is also identified in petrography as disseminated crystals. The presence of pyrite had already been described for the Guia Formation (Romero *et al.* 2013).

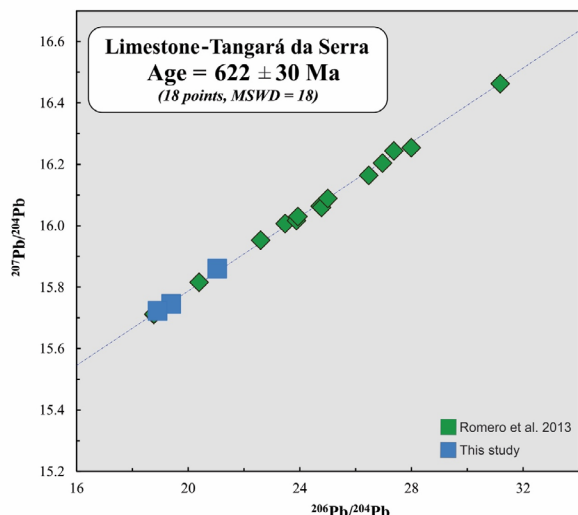


**Figure 7.**  $^{207}\text{Pb}/^{204}\text{Pb}$  vs.  $^{206}\text{Pb}/^{204}\text{Pb}$  diagram for the limestone of the cap carbonate of Tangará da Serra. The samples analyzed by Romero *et al.* (2013) are in green. In blue are the results of the total dissolution of the three samples TS-080, TS-107, and TS-121 (this study).

**Table 3.** Sr isotopic analyses for carbonate samples by sequential leaching steps (L1–L9) from this work and from Romero *et al.* (2013) (CT3-11). The values used to calculate the weighted average of  $^{87}\text{Sr}/^{86}\text{Sr}$  ratios for each sample are shown in italics and bold. Values in parentheses are uncertainty at  $\pm 2\sigma$  ( $10^{-6}$ ).

Aliquot	L1	L2	L3	L4	L5	L6	L7	L8	L9	Mean
Sample	$^{87}\text{Sr}/^{86}\text{Sr}$									
TS-125	0.707642 (30)	<b>0.707552</b> (22)	<b>0.707411</b> (29)	<b>0.707519</b> (26)	0.707580 (30)	0.707884 (21)	0.707635 (28)	–	–	<b>0.707548</b> (69)
TS-121	0.707703 (27)	0.707908 (26)	–	–	<b>0.707358</b> (24)	0.707885 (32)	0.707577 (39)	<b>0.707388</b> (34)	<b>0.707354</b> (44)	<b>0.707366</b> (42)
TS-114	0.707785 (21)	0.707749 (12)	0.707742 (23)	<b>0.707705</b> (36)	<b>0.707682</b> (27)	<b>0.707693</b> (20)	<b>0.707708</b> (25)	–	–	<b>0.707696</b> (12)
TS-107	0.709885 (80)	0.708219 (27)	–	–	–	–	–	<b>0.707595</b> (24)	–	<b>0.707595</b> (24)
TS-093	0.707379 (05)	0.707303 (5)	0.707279 (5)	0.707265 (3)	0.707289 (6)	0.707299 (5)	<b>0.707224</b> (15)	–	–	<b>0.707224</b> (15)
TS-080	0.707538 (72)	<b>0.707392</b> (43)	<b>0.707340</b> (53)	0.707537 (28)	0.707606 (25)	0.707486 (28)	0.707660 (48)	0.707444 (29)	<b>0.707355</b> (30)	<b>0.707362</b> (57)
TS-073	0.707252 (23)	0.707374 (26)	<b>0.707191</b> (19)	<b>0.707223</b> (25)	<b>0.707201</b> (23)	<b>0.707157</b> (23)	0.707250 (24)	–	–	<b>0.707192</b> (41)
TS-069	0.707739 (42)	0.707717 (28)	<b>0.707501</b> (36)	<b>0.707538</b> (31)	0.707751 (39)	<b>0.707568</b> (41)	0.707741 (27)	0.708231 (25)	–	<b>0.707534</b> (77)
TS-060	0.70742 (87)	0.707455 (61)	0.707550 (70)	0.707490 (74)	<b>0.707263</b> (64)	0.707397 (37)	<b>0.707247</b> (37)	0.707312 (31)	–	<b>0.707251</b> (31)
TS-056	0.707396 (91)	0.707295 (20)	<b>0.707073</b> (67)	0.706875 (99)	0.706969 (94)	<b>0.707078</b> (74)	0.707386 (76)	0.707972 (48)	–	<b>0.707075</b> (49)
TS-050	0.707181 (23)	<b>0.707068</b> (34)	0.707133 (19)	<b>0.707049</b> (23)	<b>0.707047</b> (20)	<b>0.707043</b> (32)	<b>0.707053</b> (24)	–	–	<b>0.707051</b> (11)
CT3-11	<b>0.707098</b> (26)	<b>0.707060</b> (45)	<b>0.707025</b> (41)	<b>0.707097</b> (25)	<b>0.707116</b> (33)	<b>0.707056</b> (90)	0.707163 (34)	–	–	<b>0.707088</b> (31)

**Table 4.** Sm-Nd isotopic data for the carbonate samples of the Guia Formation, at the Calcário Tangará Quarry.

Sample	Sm <sub>(ppm)</sub>	Nd <sub>(ppm)</sub>	<sup>147</sup> Sm/ <sup>144</sup> Nd	2σ	<sup>143</sup> Nd/ <sup>144</sup> Nd	2σ	f(Sm-Nd)	ε <sub>Nd(635Ma)</sub>	T <sub>(DM)</sub> (Ga)
TS-125	0.98	4.34	0.1365	0.0041	0.512042	0.000081	-0.31	-6.7	1.98
TS-121	1.01	4.51	0.1354	0.0014	0.511935	0.000051	-0.31	-8.8	2.16
TS-114	0.98	4.22	0.1408	0.0088	0.511838	0.000080	-0.28	-11.1	2.54
TS-107	1.89	7.81	0.1460	0.0023	0.512055	0.000026	-0.26	-7.3	2.23
TS-093	1.03	4.59	0.1364	0.0020	0.511932	0.000028	-0.31	-8.9	2.20
TS-080	1.06	4.78	0.1337	0.0029	0.512060	0.000047	-0.32	-6.2	1.87
TS-073	1.14	5.19	0.1328	0.0012	0.511976	0.000045	-0.32	-7.7	2.01
TS-069	1.30	5.76	0.1369	0.0043	0.511965	0.000052	-0.30	-8.3	2.14
TS-060	0.89	4.04	0.1334	0.0015	0.511887	0.000054	-0.32	-9.5	2.20
TS-056	1.31	5.65	0.1398	0.0025	0.512060	0.000030	-0.29	-6.7	2.03
TS-050	0.84	3.77	0.1339	0.0020	0.511921	0.000045	-0.32	-8.9	2.15
CT3-11	0.87	3.73	0.1416	0.0048	0.512167	0.000068	-0.28	-4.7	1.85

## Lead-Lead dating

The age of  $622 \pm 30$  Ma obtained together with data from Romero *et al.* (2013) for the limestones of the studied section of the Guia Formation (Fig. 7) represents a complementary contribution to the Pb-Pb age of  $622 \pm 33$  Ma established by these authors, slightly improving the accuracy. This age agrees with the Pb-Pb age of  $627 \pm 32$  Ma, which was obtained by Babinski *et al.* (2006) for the same cap carbonate in the Mirassol d'Oeste region, and reinforces that the cap carbonate of the Araras Group is surely related to the Marinoan glaciation.

## Sr isotopic evidence of continental contribution

### *Intra-sample variations of Sr isotopic signature*

According to Bailey *et al.* (2000), the sequential leaching procedure with weak and diluted acid allows for the minimization of the influence of Sr removed from terrigenous materials with a more radiogenic <sup>87</sup>Sr/<sup>86</sup>Sr ratio that modifies the Sr isotopic signature of the carbonate phase. The non-removal of these higher values prevents any confident interpretation of the <sup>87</sup>Sr/<sup>86</sup>Sr ratio as a primary Sr isotopic signature of the carbonates. The carbonates from the Calcário Tangará Quarry show important variations of the <sup>87</sup>Sr/<sup>86</sup>Sr ratio between the aliquots of the same sample. These internal variations cannot be attributed to the contribution of terrigenous material because the sequential leaching procedure is supposed to avoid remobilizing Sr from siliciclastic material.

Normally, the first aliquot (L1) has a higher value than the others because it contains Sr radiogenic from the environment incorporated after the carbonate precipitation. This behavior was observed in samples TS-50 and TS-093. Likewise, the last aliquots often have a more radiogenic isotope ratio probably due to the removal of some Sr from siliciclastic minerals. For instance, samples TS-056 and TS-069 showed this behavior. However, in most samples, these simple behaviors were not identified and some random variations of the <sup>87</sup>Sr/<sup>86</sup>Sr ratio were found at different intermediary leaching steps. These internal variations could be explained by an isotopic heterogeneity of Sr dissolved in water during the precipitation of carbonates or by

the incorporation of radiogenic Sr during diagenesis. The former hypothesis seems more likely because, in all samples, the presence of the siliciclastic material has been detected, indicating an influence of the continent. Unfortunately, it is not possible here to conclude about the origin of such intra-sample variations of the <sup>87</sup>Sr/<sup>86</sup>Sr ratio without a more specific investigation such as a detailed geochemical study of each leached phase or *in situ* isotopic/geochemical analyses by ICP-MS with laser ablation. This behavior is poorly documented in the literature. In Cryogenian and Ediacaran cap carbonates from Australia, slight internal variations in the <sup>87</sup>Sr/<sup>86</sup>Sr ratio in some samples were interpreted as a complex combination of contributions from clay minerals, post-depositional carbonates, and primary carbonates with variable <sup>87</sup>Sr/<sup>86</sup>Sr ratios (Verdel *et al.* 2018). Alternatively mixing between crystal fans and micritic matrix with slightly different Sr isotopic signatures may also account for the intrasample <sup>87</sup>Sr/<sup>86</sup>Sr variations (see Caxito *et al.* 2021). Regardless of the origin of these internal variations, the weighted average of the lowest values of the <sup>87</sup>Sr/<sup>86</sup>Sr ratio between the aliquots is interpreted here as the primary Sr isotopic signature of the seawater at the time of the carbonate precipitation.

### *Sr isotopic variation in the samples along the section*

From one sample to another, variations in the <sup>87</sup>Sr/<sup>86</sup>Sr ratio generally occur at the fourth decimal place. Although these variations occur in a restricted range, they must be considered significant when the isotopic ratios do not overlap within the error. According to Romero *et al.* (2013), the variations can be explained either because of diagenetic processes or by the contribution of radiogenic Sr from terrigenous. Petrography indicates that the diagenetic processes were not strongly active and there is no relationship between the degree of diagenetic transformation and the variation of the <sup>87</sup>Sr/<sup>86</sup>Sr ratio from one sample to another. So, diagenesis seems unable to explain the differences in the <sup>87</sup>Sr/<sup>86</sup>Sr ratio between the samples. On the contrary, it was possible to observe a large amount of terrigenous grains ranging from ~5% to ~20% of the total weight of the samples (Fig. 8). Throughout the profile, there is an increase in both the <sup>87</sup>Sr/<sup>86</sup>Sr ratio and the amount of terrigenous,

suggesting a possible correlation. Romero *et al.* (2013) also identified the occurrence of terrigenous grains in the carbonate samples, but without having quantified their abundance. These authors showed that higher  $\text{SiO}_2$ ,  $\text{Al}_2\text{O}_3$ ,  $\text{Fe}_2\text{O}_3$ ,  $\text{K}_2\text{O}$ , and Rb contents occur in samples that present terrigenous grains forming thin layers. They also established a correlation between the isotopic signature and the abundances of major oxides ( $\text{SiO}_2$ ,  $\text{Al}_2\text{O}_3$ , and  $\text{K}_2\text{O}$ ) and attributed the control of the  $^{87}\text{Sr}/^{86}\text{Sr}$  ratio to the terrestrial contribution. However, although there is an increasing trend of the abundance of terrigenous materials and the  $^{87}\text{Sr}/^{86}\text{Sr}$  ratio, their variation is clearly decoupled. Samples with higher  $^{87}\text{Sr}/^{86}\text{Sr}$  ratios are not those that display higher amounts of terrigenous minerals (Fig. 8). The leaching procedure indicates that the isotopic signature comes from the carbonate phase and does not originate from the terrigenous material. Consequently, this isotopic signature must have its origin in Sr dissolved in ocean water that was incorporated into carbonates when they precipitated. Therefore, it is suggested that an increase in the Sr isotopic signature and the percentage of siliciclastic material both have a continental origin and point to an increase in the continental contribution through transported material (terrigenous) and dissolved material (dissolved Sr) of the melting water from rivers.

The  $^{87}\text{Sr}/^{86}\text{Sr}$  ratios between 0.7070 and 0.7077 from this study agree with those of Romero *et al.* (2013), considering their progressive increase along the profile. They also support the explanation advanced by Romero *et al.* (2013) concerning the data by Nogueira *et al.* (2007) and Alvarenga *et al.* (2008), which represent a signature with a contribution of radiogenic Sr probably leached from siliciclastic minerals rather than the primary signature of seawater. This reinforces the importance of using a procedure such as that of Bailey *et al.* (2000), in order

to ensure that the signature from only the carbonate phase is being determined.

Soares and Nogueira (2008) identified a deepening of the platform where the Guia Formation deposited, suggesting that the carbonates formed in this environment would gradually move away from continental sources. Then, a decrease of the  $^{87}\text{Sr}/^{86}\text{Sr}$  ratios should therefore be expected. However, data from this study and Romero *et al.* (2013) indicate that the continental contribution during the formation of carbonates continued to increase rapidly along the profile. Despite the deepening of the basin, this increase in the Sr isotopic ratio suggests that the intensity of continental weathering has increased independently of the basin distance and depth. Such behavior is in better agreement with the “weathering” model proposed by Hoffman *et al.* (2017), which suggested that the ocean alkalinity was controlled by intense weathering, resulting in the formation of the Marinoan cap carbonate.

The Guia Formation is overlain by the Serra do Quilombo and Nobres formations, which also show an increase in the isotopic composition of Sr. While, in the Guia Formation, the  $^{87}\text{Sr}/^{86}\text{Sr}$  ratio ranges from 0.7070 to 0.7077, it ranges from 0.7082 to 0.7085 in the Serra do Quilombo Formation and from 0.7085 to 0.7088 in the Nobres Formation (Nogueira *et al.* 2019). These progressively higher  $^{87}\text{Sr}/^{86}\text{Sr}$  values attest to the progressive increase in the continental contribution throughout the whole profile of the Araras Group.

#### Comparison with Marinoan cap carbonates worldwide

After the Marinoan glaciation, the carbonate layers worldwide were deposited in a short period. In modern analogs, Font *et al.* (2010) deduced a very fast sedimentation rate that could also apply to Marinoan cap carbonates. This means that the

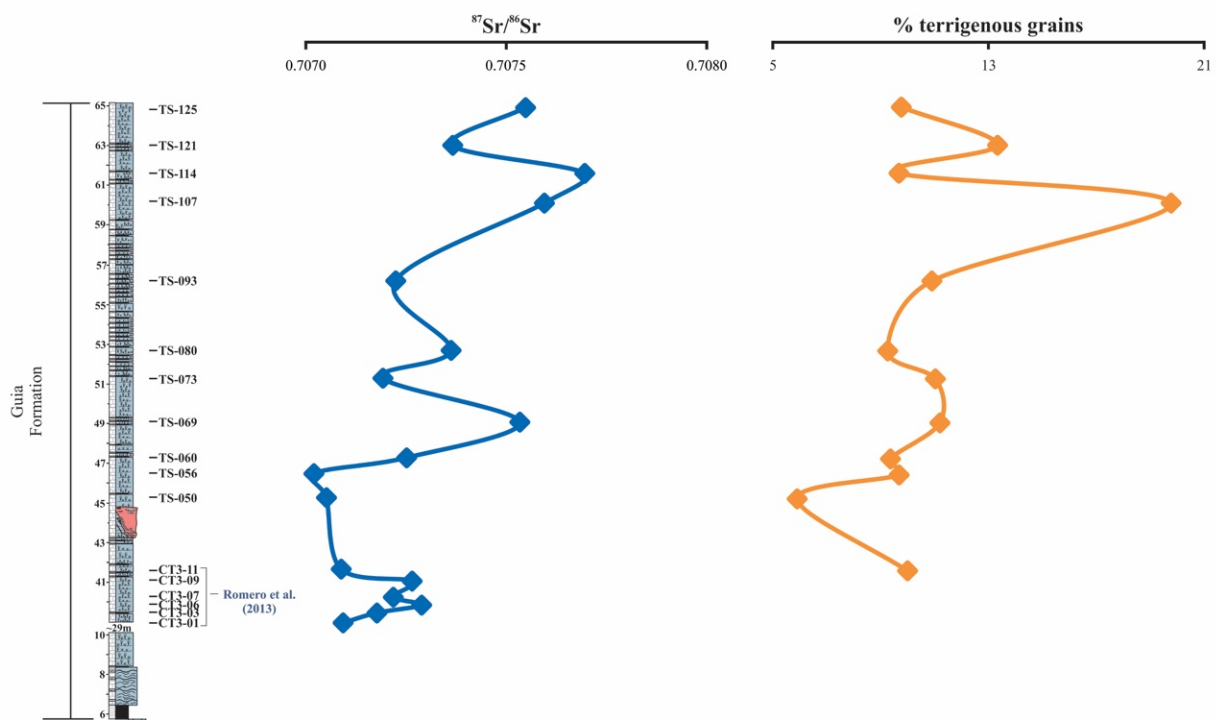


**Figure 8.** Variation of Sr isotopic composition and percentage of terrigenous grains in the samples along the section of the Guia Formation at Calcário Tangará Quarry. Sr isotopic data from Romero *et al.* (2013) are also reported.

increase in the  $^{87}\text{Sr}/^{86}\text{Sr}$  ratio occurred in a very short time, with a sedimentation time for the Marinoan carbonate layers of less than 1 Ma, on the order of a few hundred thousand years. Then the increase in the  $^{87}\text{Sr}/^{86}\text{Sr}$  ratio along the Calcário Tangará Quarry section indicates a sudden change in the characteristics of seawater due to the progressive increase in the contribution of continental material as the thaw occurs, bringing Sr from river water together with terrigenous material, that is, an important influx of radiogenic Sr dissolved in river waters.

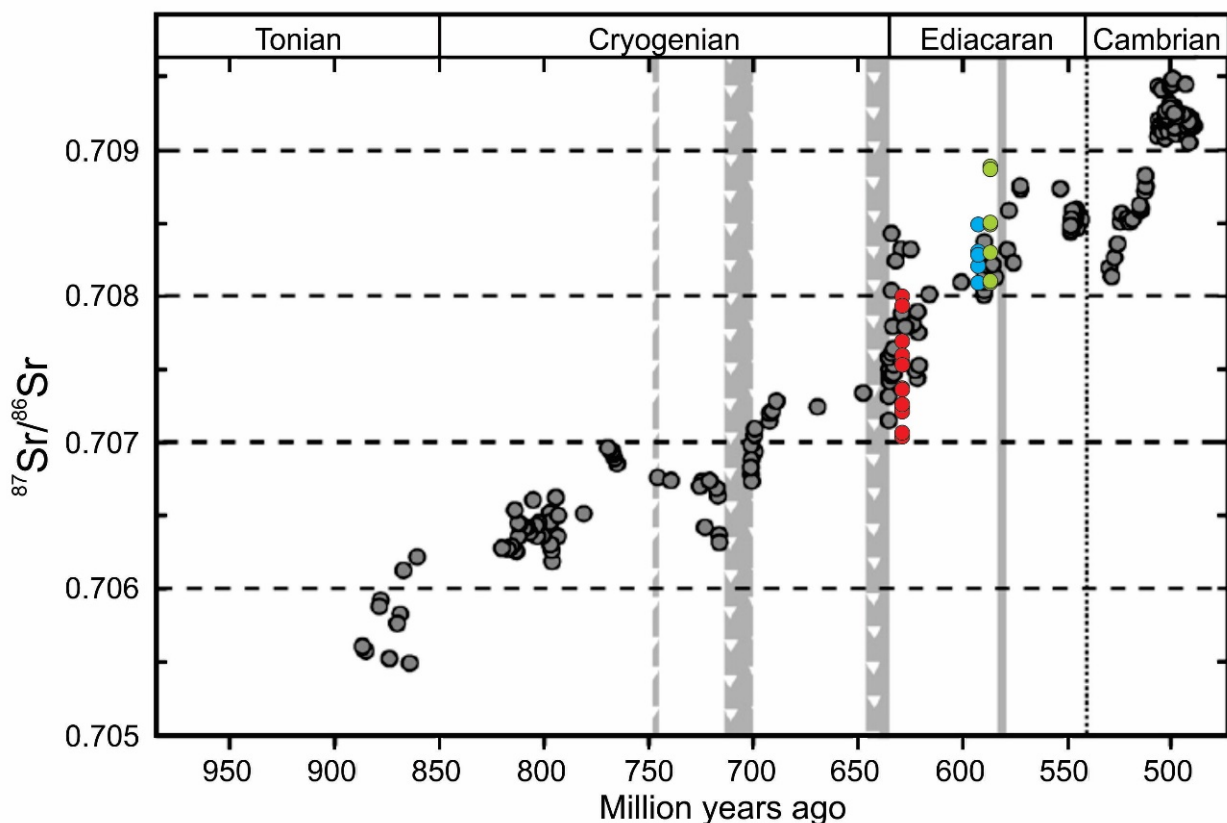
On a global scale, Sr isotopic data on marine carbonate rocks were used to establish the Sr evolution of seawater during the Neoproterozoic. This evolution is represented by different curves that have been compiled by Melezhik *et al.* (2001) and depicts the complex behavior of the Sr isotopic signatures during the Neoproterozoic, especially at the Cryogenian/Ediacaran transition. However, all curves indicated an abrupt increase shortly after the Marinoan glaciation. Halverson *et al.* (2007) pointed out two processes for such an abrupt increase: stratification of the ocean between the ocean floor and its surface, with the composition of Sr highly influenced in the latter by a large influx of radiogenic Sr from continental fresh waters (Shields 2005, Hurtgen *et al.* 2006) and high rates of silicate weathering resulting in a large flow of radiogenic Sr to the ocean surface (Hoffman *et al.* 1998a, Kasemann *et al.* 2005).

Among the several proposals for the Sr isotopic evolution curve of seawater over the Neoproterozoic, the values obtained in this study are in greater agreement with the curve proposed by Halverson *et al.* (2010). According to these authors,

the  $^{87}\text{Sr}/^{86}\text{Sr}$  ratio was 0.7072 at the end of the Cryogenian, which is compatible with the data by Romero *et al.* (2013) and those from this study (Fig. 9). This confirms its rapid increase shortly after the glaciation up to around 0.7080 in the second half of Ediacaran.

Sr isotopic data from more recent studies on late Cryogenian and early Ediacaran carbonate layers around the world are compiled in Fig. 10. Such formations have an age within the range of  $622 \pm 30$  Ma determined for the Guia Formation. Pre-Marinoan carbonate rocks such as the Taishir Formation, Mongolia (0.7070–0.7074) and Keele Formation, NW Canada (0.7071–0.7072) show low and constant  $^{87}\text{Sr}/^{86}\text{Sr}$  ratios. These  $^{87}\text{Sr}/^{86}\text{Sr}$  ratios of carbonate layers show wide variations right after the Marinoan glaciation, from values similar to pre-Marinoan data (Guia, Hayhook, Maieberg, and Ol formations), up to higher values close to 0.7086 (Bambui Group, in Brazil).

The data compiled in Fig. 10 were obtained by the step-leaching method with weak and diluted acid (acetic acid or ammonium acetate) for the dissolution of carbonates. Thus, no significant influence of Sr from terrigenous material on the  $^{87}\text{Sr}/^{86}\text{Sr}$  ratio is expected and these values are representative of the isotopic composition of seawater at the time and in the place where these rocks were formed. The large variation in the  $^{87}\text{Sr}/^{86}\text{Sr}$  ratio (0.7070–0.7086) immediately after the Marinoan glaciation can be explained by the increased influence of the continental waters on the oceans. According to Wei *et al.* (2019), the Sr isotopes along the sections of the Maieberg formation consistently exhibit a covariable trend in



Source: modified from Halverson *et al.* (2010).

**Figure 9.** Compilation of Sr isotopic data from Halverson *et al.* (2007, 2010), Shields (2005), Nogueira *et al.* (2007), Melezhik *et al.* (2001), and unpublished data from Milhomem Neto (2012), in the Guia (red dots; this study), Serra do Quilombo (blue dots) and Nobres (green dots) formations.

the lithological successions of the respective carbonate layers that can be well explained with a diagenetic mixing model. According to this model, the positive  $^{87}\text{Sr}/^{86}\text{Sr}$  excursion may result from the increasing influence of melted water (high  $^{87}\text{Sr}/^{86}\text{Sr}$  ratio of dissolved Sr) and runoff from newly exposed continental rocks that mix in the marine waters (low  $^{87}\text{Sr}/^{86}\text{Sr}$  ratio), right after the Marinoan glaciation. The interpretation of the Sr isotopic data of this study regarding the Guia Formation is by the proposal of Wei *et al.* (2019), involving the mixture of Sr dissolved in melting freshwater with ocean waters, and not only a Sr contribution of the terrigenous material transported by freshwater.

## Nd isotopic signature

Neodymium is incorporated into the structure of carbonates at the time of precipitation (Banner 2004). Then it records the isotopic signature and model ages of mantle extraction from the source rocks that were eroded and transported to the oceanic basin, and finally incorporated in the seawater and precipitated along with the carbonates.

The  $T_{\text{DM}}$  ages of these rocks represent the average time since their continental sources were initially extracted from the mantle (Banner 2004). Except for the TS-114 sample, which displayed a Neoproterozoic age, the  $T_{\text{DM}}$  ages are all Rhyacian to Orosirian, ranging from 1.85 to 2.23 Ga. These ages are in accordance with those of crust formation in the Maroni-Itacaiúnas (~2.0–2.5 Ga) and Ventuari-Tapajós (~1.8–2.0 Ga) provinces and the Rio Negro-Juruena province (~1.5–2.0 Ga) of the Amazonian Craton (Cordani and Sato 1999). However, it cannot be excluded that the  $T_{\text{DM}}$  ages reflect the contribution of other nearby sources, such as rocks from the Sunsás Province, because their  $T_{\text{DM}}$  ages are within the same range as these older provinces in the Amazon Craton (Cordani and Sato 1999, Santos *et al.* 2008). Furthermore, considering the great distance of the Maroni-Itacaiúnas province from the Tangará da Serra area, it cannot be excluded that the Rhyacian TDM ages may represent mixing ages between an older and closer source, such as the Carajás Province (~3.0 ± 0.1 Ga; Feio *et al.* 2013) and sources from the other younger

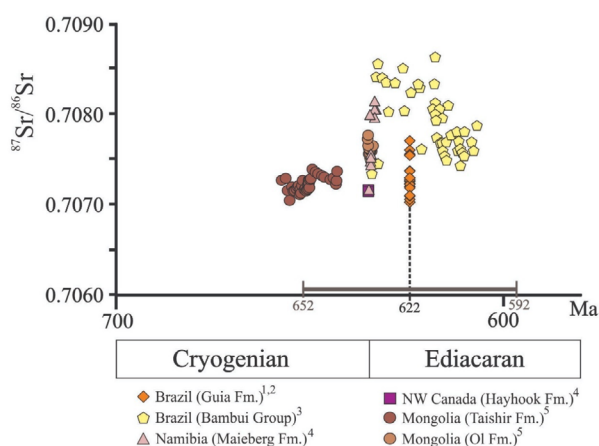
provinces. Such a crust constitutes the basement of the Guia Formation and probably the continental crustal source from the sediments transported by the river waters. The  $\epsilon_{\text{Nd}}$  values were all negative, from -11.1 to -4.7, and these data suggest that the Nd dissolved in water and precipitated in carbonates and/or the siliciclastic minerals originates from an old crust. Unlike Sr, the isotopic ratio of which tends to increase along the section, the Nd isotopic compositions vary rapidly and randomly to more or less radiogenic values, with great amplitude (Fig. 11). However, as the dissolution was done with strong acid, it cannot be asserted that the seawater Nd isotopic composition is changing, because the terrigenous minerals may also play an important role in the Nd isotopic compositions of the carbonate rocks.

The TS-114 sample is the only one that showed agreement between the Sr and Nd data, with the highest  $^{87}\text{Sr}/^{86}\text{Sr}$  ratio (0.7077), together with the lowest value of  $\epsilon_{\text{Nd}}$  (-11.1) and the oldest  $T_{\text{DM}}$  age (2.54 Ga). The non-correlation between Sr and Nd isotopic data for most samples may be linked to different types of contribution: in the case of Sr, it would be dissolved in seawater, and in the case of Nd, from siliciclastic material or mixing of both contributions.

Dantas *et al.* (2009) performed Sm-Nd analyses in Neoproterozoic sedimentary rocks of the Araras group and Paraguay Belt. For carbonates of the Araras Group, the  $T_{\text{DM}}$  ages are between 1.74 and 2.11 Ga, and  $\epsilon_{\text{Nd}}$  values (calculated at 600 Ma) are between -8.2 and -11.4, which suggests an old continental source. Similar isotopic signatures were obtained for glacial rocks in the successions studied by Dantas *et al.* (2009), which led the authors to infer a rapid rate of precipitation of the carbonates and that their isotopic composition was strongly influenced by the Amazonian craton basement.

In modern seawater, the Nd isotopic composition is highly variable, with  $\epsilon_{\text{Nd}}$  values from 0 to -25 (Van de Flieddt *et al.* 2016). Isotopic variations of Nd can be used to relate the residence time of Nd and mixing rates between the oceans (Piepgras and Wasserburg 1980). How seawater acquires its Nd isotopic composition is not yet fully resolved, due to the complex behavior of the Sm-Nd system and the short residence time of Nd in aquatic compartments. Hydrothermal vents in the deep ocean may influence the isotopic and mass balance of Nd in the oceans. However, it is accepted that a clear relationship exists between the presence of Nd in seawater and continental inputs, whether from river water or suspended sediments (Jeandel *et al.* 2007, 2013).

Regarding the Nd isotopic composition from the Neoproterozoic oceans, Keto and Jacobsen (1988) proposed “The global average paleoceanic  $\epsilon_{\text{Nd}}$  curve” for the last 800 Ma, where the  $\epsilon_{\text{Nd}}$  varies from -1 to -10 Ma between 650 and 600 Ma. Jiedong *et al.* (1997) obtained  $\epsilon_{\text{Nd}}$  values between -4.5 and -8.0 for Chinese seawater during the Neoproterozoic through phosphatic sedimentary rocks and Manganese deposits. Condie and Aster (2013) reported the Nd and Sr isotopic evolution curves for seawater at a global scale from Neoproterozoic to Cretaceous, according to Keto and Jacobsen (1988) and Shields (2007), respectively.



Source: (1) This study, (2) Romero *et al.* (2013), (3) Caxito *et al.* (2021), (4) Halverson *et al.* (2007), (5) Bold *et al.* (2016).

**Figure 10.** Compilation of data from the  $^{87}\text{Sr}/^{86}\text{Sr}$  ratio to the end of Cryogenician—beginning of Ediacaran around the world.

The  $\epsilon_{Nd}$  values of the samples from the Guia Formation and those of Dantas *et al.* (2009) at the time of deposition, with average values of  $-7.9 \pm 1.7$  and  $-10.0 \pm 1.2$ , respectively, are in agreement with the Nd isotopic curve estimated for early Ediacaran seawater (Fig. 12). Thus, it can be admitted that the carbonates of the Guia Formation portray the isotopic composition of Nd from seawater at the time they were precipitated.

### CONCLUSIONS

The petrographic and Pb-Sr-Nd isotopic study of the rocks of the upper portion of the Guia Formation in the region of Tangará da Serra allowed us to draw the following conclusions for the Marinoan cap carbonate in the south of the Amazonian Craton:

The Pb-Pb age of  $622 \pm 30$  Ma consolidated the age previously obtained by Romero *et al.* (2013), slightly improving its accuracy and reinforcing the relationship of the Guia Formation with the Marinoan glaciation.

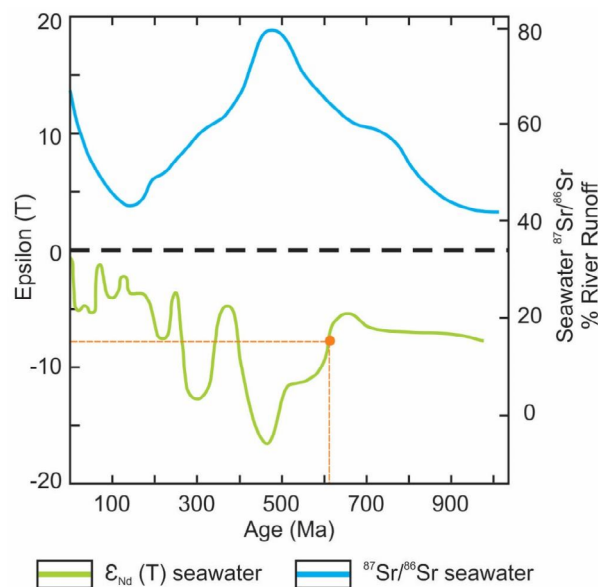
The continental influence on the ocean waters from which the carbonates of the Guia Formation precipitated was evidenced by all the methods used.

The petrographic study and X-ray diffraction allowed us to identify quartz, mica, and feldspar as the terrigenous materials disseminated in the rocks, in addition to diagenetic characteristics that may have facilitated the introduction of material coming from the continent during or after the precipitation of carbonates. An increase in the amount of siliciclastic material was evidenced throughout the profile studied, indicating an increase in the contribution of suspended material brought by continental waters.

An increasing continental contribution from dissolved Sr of freshwater is also evidenced by the  $^{87}\text{Sr}/^{86}\text{Sr}$  ratios in the carbonate phase of the samples which grew from 0.7070 to 0.7077 along the profile. This rapid increase in the Sr isotopic signature after the Marinoan glaciation indicates that mixing

processes between ocean and continental waters were intense. This abrupt increase in the  $^{87}\text{Sr}/^{86}\text{Sr}$  ratio (0.7070–0.7086) at the Cryogenian–Ediacaran transition is registered in post-Marinoan carbonate in different parts of the world, which can be explained by the increased continental influence in the ocean. The large variations of the  $^{87}\text{Sr}/^{86}\text{Sr}$  ratios on a global scale indicate that the ocean waters did not reach homogeneity of the Sr isotopic signature during Ediacaran.

The  $\epsilon_{Nd(635\text{Ma})}$  values, between -4.7 and -11.1, indicate the presence of Nd from suspended material transported from continents to seawater from which the carbonates precipitated. The  $T_{DM}$  ages between 1.84 and 2.54 Ga suggest that the continental sources are the Paleoproterozoic provinces of the



Source: modified from Condie and Aster (2013).

**Figure 12.** Compilation of Sr and Nd isotopic compositions in seawater along the Neoproterozoic and Phanerozoic. The mean value of  $\epsilon_{Nd}$  seawater at 622 Ma is represented in orange, which was found similar to those of the samples of this study.

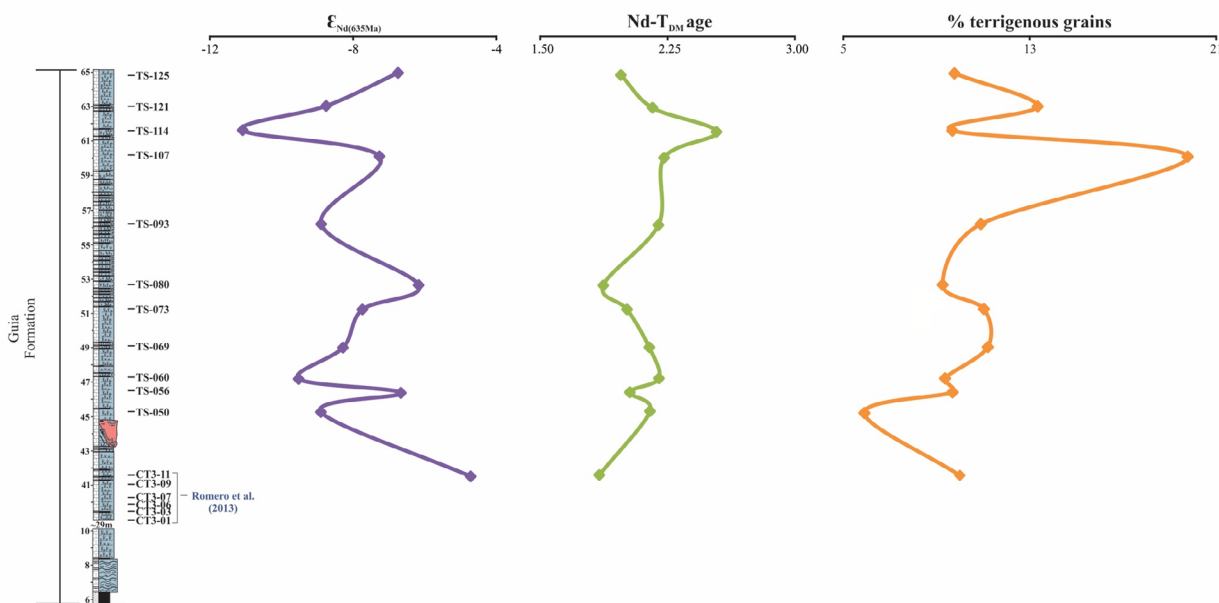


**Figure 11.** Variation of  $\epsilon_{Nd(635\text{Ma})}$ ,  $T_{DM}$  age, and percentage of terrigenous grains in the samples along the section of the Guia Formation at Calcário Tangará Quarry.

Amazonian Craton. As for Sr, the random variations of  $T_{DM}$  ages and  $\epsilon_{Nd}$  values suggest important and rapid variations in the continental contribution to the post-Marinoan carbonates of the Araras Group.

## ACKNOWLEDGMENTS

We acknowledge the Brazilian National Council for Scientific and Technological Development (CNPq) for

granting a master scholarship to the first author (Process No. 133936/2013-9), and a research scholarship to J.M. Lafon (Process No. 312393/2020-2). The authors are grateful to Dr. Rômulo Angélica for the analysis in the LCM laboratory (UFPA) and Dr. Afonso Nogueira for the support provided through the petrographic laboratory of the GSED research group. Additionally, the authors thank Dr. Fabricio Caxito and an anonymous reviewer for their helpful comments that greatly improved our manuscript.

## ARTICLE INFORMATION

Manuscript ID: 20230015. Received on: 24 APRIL 2022. Approved on: 01 DEC 2023.

How to cite: Souza N.M.C., Lafon J.M., Milhomem Neto J.M., Soares J.L. (2023). Continental contribution to the marinoan cap carbonate of Tangará da Serra – MT, Brazil: further evidence from Sr-Nd-Pb isotope geochemistry. *Brazilian Journal of Geology*, 54(1):e20230015. <https://doi.org/10.1590/2317-4889202420230015>

N.M.C.S.: Conceptualization, Methodology, Writing – original draft, Writing – review & editing. J.M.L.: Conceptualization, Funding acquisition, Methodology, Validation, Writing – original draft, Writing – review & editing. J.M.M.N.: Conceptualization, Formal Analysis, Methodology, Supervision, Validation, Visualization, Writing – review & editing. J.L.S.: Writing – original draft, writing – review & editing, Investigation.

## REFERENCES

- Almeida F.F.M., Hasui Y. 1984. *O Pré-Cambriano do Brasil*. São Paulo: Edgard Blucher, 378 p.
- Alvarenga C.J.S., Dardenne M.A., Santos R.V., Brod E.R., Gioia S.C.L., Sial A.N., Dantas E.L., Ferreira V.P. 2008. Isotope stratigraphy of Neoproterozoic cap carbonates in the Araras Group, Brazil. *Gondwana Research*, 13(4):469-479. <https://doi.org/10.1016/j.gr.2007.05.004>
- Alvarenga C.J.S., Santos R.V., Vieira L.C., Lima B.A.F., Mancini L.H. 2014. Meso-Neoproterozoic isotope stratigraphy on carbonates platforms in the Brasília Belt of Brazil. *Precambrian Research*, 251:164-180. <https://doi.org/10.1016/j.precamres.2014.06.011>
- Babinski M., Trindade R.I.F., Alvarenga J.C., Boggiani P.C., Liu D., Santos R.V. 2006. Geochronological constraints on the Neoproterozoic glaciations in Brazil. *Snowball Earth*, 1:19-20.
- Bailey T.R., McArthur J.M., Prince H., Thirlwall M.F. 2000. Dissolution methods for strontium isotope stratigraphy: whole rock analysis. *Chemical Geology*, 167(3-4):313-319. [https://doi.org/10.1016/S0009-2541\(99\)00235-1](https://doi.org/10.1016/S0009-2541(99)00235-1)
- Bandeira J., McGee B., Nogueira A.C.R., Collins A.S., Trindade R. 2012. Sedimentological and provenance response to Cambrian closure of the Clymene ocean: The upper Alto Paraguai Group, Paraguay belt, Brazil. *Gondwana Research*, 21:323-340. <https://doi.org/10.1016/j.gr.2011.04.006>
- Bandeira J., Nogueira A.C.R., Petri S., Riccomini C., Trindade R.I.F., Sial A.N., Ridalga R.L. 2007. Depósitos litorâneos neoproterozóicos do Grupo Alto Paraguai no sudoeste do Cráton Amazônico, região de Mirassol d'Oeste, Mato Grosso. *Revista Brasileira de Geociências*, 37(3):595-606.
- Banner J.L. 2004. Radiogenic isotopes: systematics and applications to earth surface processes and chemical stratigraphy. *Earth-Science Reviews*, 65(3-4):141-194. [https://doi.org/10.1016/S0012-8252\(03\)00086-2](https://doi.org/10.1016/S0012-8252(03)00086-2)
- Barreto C.J.S., Lafon J.M., Rosa Costa L.T., Lima E.F. 2014. Palaeoproterozoic (~1.89 Ga) felsic volcanism of the Iricoume Group, Guyana Shield, South America: geochemical and Sm-Nd isotopic constraints on sources and tectonic environment. *International Geology Review*, 56(11):1332-1356. <https://doi.org/10.1080/00206814.2014.930800>
- Bold U., Smith E.F., Rooney A.D., Bowring S.A., Buchwaldt R., Dúdás F.O., Ramezani J., Crowley J.L., Schrag D.P., Macdonald F.A. 2016. Neoproterozoic stratigraphy of the Zavkhan terrane of Mongolia: the backbone for Cryogenian and early Ediacaran chemostratigraphic records. *American Journal of Science*, 316(1):1-63. <https://doi.org/10.2475/01.2016.01>
- Caxito F., Lana C., Frei R., Uhlein G.J., Sial A.N., Dantas E.L., Pinto A.G., Campos F.C., Galvão P., Warren L.V., Okubo J., Ganade C.E. 2021. Goldilocks at the dawn of complex life: mountains might have damaged Ediacaran–Cambrian ecosystems and prompted an early Cambrian greenhouse world. *Scientific Reports*, 11:20010. <https://doi.org/10.1038/s41598-021-99526-z>
- Caxito F.A., Halverson G.P., Uhlein A., Stevenson R., Dias T.C., Uhlein G.J. 2012. Marinoan glaciation in east central Brazil. *Precambrian Research*, 200-203:38-58. <https://doi.org/10.1016/j.precamres.2012.01.005>
- Condie K.C., Aster R.C. 2013. Refinement of the supercontinent cycle with Hf, Nd, and Sr isotopes. *Geoscience Frontiers*, 4(6):667-680. <https://doi.org/10.1016/j.gsf.2013.06.001>
- Condon D., Zhu M., Bowring S., Wang E., Yang A., Jin Y. 2005. Neoproterozoic Doushantuo Formation, China. *Science*, 308(5718):95-98. <https://doi.org/10.1126/science.1107765>
- Cordani U.G., Sato K. 1999. Crustal evolution of the South American Platform, based on Nd isotopic systematics on granitoid rocks. *Episodes*, 22(3):167-173. <https://doi.org/10.18814/epiuiugs/1999/v22i3/003>
- Dantas E.L., Alvarenga C.J.S., Santos R.V., Pimentel M.M. 2009. Using Nd isotopes to understand the provenance of sedimentary rocks from a continental margin to a foreland basin in the Neoproterozoic Paraguay Belt, Central Brazil. *Precambrian Research*, 170(1-2):1-12. <https://doi.org/10.1016/j.precamres.2008.11.005>
- DePaolo D.J. 1981. Neodymium isotopes in the Colorado Front Range and crust-mantle evolution in the Proterozoic. *Nature*, 291:193-196. <https://doi.org/10.1038/291193a0>
- Dunham R.J. 1962. Classification of carbonate rocks according to depositional texture. In: Ham W.E. (Ed.). *Classification of carbonate rocks*. American Association of Petrology and Geology, 1:21-108.
- Feio G.R.L., Dall'Agnol R., Dantas E.L., Macambira M.J.B., Santos J.O.S., Althoff F.J., Soares J.E.B. 2013. Archean granitoid magmatism in the Canaã dos Carajás area: implications for crustal evolution of the Carajás province, Amazonian craton, Brazil. *Precambrian Research*, 227:157-185. <https://doi.org/10.1016/j.precamres.2012.04.007>
- Flügel E. 2004. *Microfacies of Carbonate Rocks Analysis: Interpretation and Application*. New York: Springer Berlin Heidelberg, 976 p.

- Font E., Nédélec A., Trindade R.I.F., Moreau C. 2010. Fast or slow melting of the Marinoan snowball Earth? The cap dolostone record. *Palaeogeography, Palaeoclimatology, Palaeoecology*, **295**(1-2):215-225. <https://doi.org/10.1016/j.palaeo.2010.05.039>
- Halverson G.P., Dudás F.O., Maloof A.C., Bowring S.A. 2007. Evolution of the <sup>87</sup>Sr/<sup>86</sup>Sr composition of Neoproterozoic seawater. *Palaeogeography, Palaeoclimatology, Palaeoecology*, **256**(3-4):103-129. <https://doi.org/10.1016/j.palaeo.2007.02.028>
- Halverson G.P., Wade B.P., Hurtgen M.T., Barovich K.M. 2010. Neoproterozoic chemostratigraphy. *Precambrian Research*, **182**(4):337-350. <https://doi.org/10.1016/j.precamres.2010.04.007>
- Higgins J.A., Schrag D.P. 2003. Aftermath of a snowball Earth. *Geochemistry, Geophysics, Geosystems*, **4**(3):1028. <https://doi.org/10.1029/2002GC000403>
- Hoffman P.F., Abbot D.S., Ashkenazy Y., Benn D.I., Brocks J.J., Cohen P.A., Cox G.M., Creveling J.R., Donnadieu Y., Erwin D.H., Fairchild I.J., Ferreira D., Goodman J.C., Halverson G.P., Jansen M.F., Le Hir G., Love G.D., Macdonald F.A., Maloof A.C., Partin C.A., Ramstein G., Rose B.E.J., Rose C.V., Peter M., Sadler P.M., Tziperman E., Voigt A., Warren S.G. 2017. Snowball Earth climate dynamics and Cryogenian geology-geobiology. *Science Advances*, **3**(11):e1600983. <https://doi.org/10.1126/sciadv.1600983>
- Hoffman P.F., Kaufman A.J., Halverson G.P. 1998a. Comings and goings of global glaciations on a Neoproterozoic tropical platform in Namibia. *GSA Today*, **8**(5):1-9.
- Hoffman P.F., Kaufman A.J., Halverson G.P., Schrag D.P. 1998b. A Neoproterozoic Snowball Earth. *Science*, **281**(5381):1342-1346. <https://doi.org/10.1126/science.281.5381.1342>
- Hoffman P.F., Schrag D.P. 2002. The Snowball earth hypothesis: testing the limits of global changes. *Terra Nova*, **14**(3):129-155. <https://doi.org/10.1046/j.1365-3121.2002.00408.x>
- Hurtgen M., Halverson G., Arthur M., Hoffman P. 2006. Sulfur cycling in the aftermath of a Neoproterozoic (Marinoan) snowball glaciation: evidence for a syn-glacial sulfidic deep ocean. *Earth and Planetary Science Letters*, **245**(3-4):551-570. <https://doi.org/10.1016/j.epsl.2006.03.026>
- Jacobsen S.B., Kaufman A.J. 1999. The Sr, C and O isotopic evolution of Neoproterozoic seawater. *Chemical Geology*, **161**(1-3):37-57. [https://doi.org/10.1016/S0009-2541\(99\)00080-7](https://doi.org/10.1016/S0009-2541(99)00080-7)
- Jeandel C., Arsouze T., Lacan F., Téchiné P., Dutay J.-C. 2007. Isotopic Nd compositions and concentrations of the lithogenic inputs into the ocean: A compilation, with an emphasis on the margins. *Chemical Geology*, **239**(1-2):156-164.
- Jeandel C., Delattre H., Grenier M., Pradoux C., Lacan F. 2013. Rare earth element concentrations and Nd isotopes in the Southeast Pacific Ocean. *Geochemistry, Geophysics, Geosystems*, **14**(2):328-341. <https://doi.org/10.1029/2012GC004309>
- Jiedong Y., Xiancong T., Yaosong X. 1997. Nd isotopic variations of Chinese seawater during Neoproterozoic through Cambrian. *Chemical Geology*, **135**(1-2):127-137. [https://doi.org/10.1016/S0009-2541\(95\)00152-2](https://doi.org/10.1016/S0009-2541(95)00152-2)
- Kasemann S., Hawkesworth C., Prave A., Fallick A., Pearson P. 2005. Boron and calcium isotope composition in Neoproterozoic carbonate rocks from Namibia: evidence for extreme environmental change. *Earth and Planetary Science Letters*, **231**(1-2):73-86. <https://doi.org/10.1016/j.epsl.2004.12.006>
- Keto L.S., Jacobsen S.B. 1988. Nd isotopic variations of Phanerozoic paleoceans. *Earth and Planetary Science Letters*, **90**(4):395-410. [https://doi.org/10.1016/0012-821X\(88\)90138-0](https://doi.org/10.1016/0012-821X(88)90138-0)
- Kirschvink J.L. 1992. Late Proterozoic low latitude glaciation: The snowball Earth. In: Schopf J.W., Klein C. (eds). *The proterozoic biosphere: A multidisciplinary study*. Cambridge: Cambridge University Press, p. 51-52.
- Marzoli A., Renne P.R., Piccirillo E.M., Ernesto M., Bellieni G., De Min A. 1999. Extensive 200-Million-Year-Old continental flood basalts of the Central Atlantic Magmatic Province. *Science*, **284**(5414):616-618. <https://doi.org/10.1126/science.284.5414.616>
- Melezhik V.A., Gorokhov I.M., Kuznetsov A.B., Fallick A.E. 2001. Chemostratigraphy of Neoproterozoic carbonates: implications for 'blind dating'. *Terra Nova*, **13**(1):1-11. <https://doi.org/10.1046/j.1365-3121.2001.00318.x>
- Milhomem Neto J.M. 2012. *Paleoambiente e quimioestratigrafia da formação Serra do Quilombo, Neoproterozóico da Faixa Paraguai Norte, regiões de Cáceres e Nobres (MT)*. Dissertation. Instituto de Geociências, Universidade Federal do Pará, Belém, 72 p.
- Nogueira A.C.R., Riccomini C. 2006. O Grupo Araras (Neoproterozoico) na Parte Norte da Faixa Paraguai e Sul do Cráton Amazônico, Brasil. *Revista Brasileira de Geociências*, **36**(4):623-640. <https://doi.org/10.25249/0375-7536.2006364576587>
- Nogueira A.C.R., Riccomini C., Sial A.N., Moura C.A.V., Trindade R.I.F., Fairchild T.R. 2007. Carbon and Strontium Isotope Fluctuations and Paleooceanographic Changes in the Late Neoproterozoic Araras Carbonate Platform, Southern Amazon Craton, Brazil. *Chemical Geology*, **237**(1-2):168-190. <https://doi.org/10.1016/j.chemgeo.2006.06.016>
- Nogueira A.C.R., Romero G.R., Sanchez E.A.M., Domingos F.H.G., Bandeira J., Santos I.M., Pinheiro R.V.L., Soares J.L., Lafon J.M., Afonso J.W.L., Santos H.P., Rudnitski I.D. 2019. The Cryogenian-Ediacaran boundary in the Southern Amazon Craton. *Chemostratigraphy Across Major Chronological Boundaries*, **240**:89-114. <https://doi.org/10.1002/9781119382508.ch6>
- Paula-Santos G.M., Caetano-Filho S., Babinski M., Trindade R.I.F., Guacaneme C. 2017. Tracking connection and restriction of West Gondwana São Francisco Basin through isotope chemostratigraphy. *Gondwana Research*, **42**:280-305. <https://doi.org/10.1016/j.gr.2016.10.012>
- Paula-Santos G.M., Figueiredo M.F., Babinski M. 2010. Isotopic anomalies (C, O and Sr) recorded in Ediacaran carbonates from the Guia Formation, Northern Paraguay Belt, Brazil. *VII South American Symposium on Isotope Geology Brasília. Short Papers*, 309-312.
- Paz S.P.A., Kahn H., Angélica R.S. 2018. A proposal for bauxite quality control using the combined Rietveld - Le Bail - Internal Standard PXRD Method - Part 1: hkl model developed for kaolinite. *Minerals Engineering*, **118**:52-61. <https://doi.org/10.1016/j.mineng.2018.01.006>
- Piegras D.J., Wasserburg G.J. 1980. Neodymium isotopic variations in seawater. *Earth and Planetary Science Letters*, **50**(1):128-138. [https://doi.org/10.1016/0012-821X\(80\)90124-7](https://doi.org/10.1016/0012-821X(80)90124-7)
- Platzner I., Ehrlich S., Halicz L. 2001. Isotope-ratio measurements of lead in NIST standard reference materials by multiple-collector inductively coupled plasma mass spectrometry. *Fresenius' Journal of Analytical Chemistry*, **370**(5):624-628. <https://doi.org/10.1007/s002160100875>
- Prave A.R., Condon D.J., Hoffmann K.H., Tapster S., Fallick A.E. 2016. Duration and nature of the end-Cryogenian (Marinoan) glaciation. *Geology*, **44**(8):631-634. <https://doi.org/10.1130/G38089.1>
- Romero J.A.S., Lafon J.M., Nogueira A.C.R., Soares J.L. 2013. Sr isotope geochemistry and Pb-Pb geochronology of the Neoproterozoic cap carbonates, Tangará da Serra, Brazil. *International Geology Review*, **55**(2):185-203. <https://doi.org/10.1080/00206814.2012.692517>
- Rudnitski I.D., Romero G.R., Hidalgo R., Nogueira A.C.R. 2016. High frequency peritidal cycles of the upper Araras Group: Implications for disappearance of the neoproterozoic carbonate platform in southern Amazon Craton. *Journal of South American Earth Sciences*, **65**:67-78. <https://doi.org/10.1016/j.jsames.2015.11.006>
- Sansjofre P., Trindade R.I.F., Ader M., Soares J.L., Nogueira A.C.R., Tribovillard N. 2014. Paleoenvironmental reconstruction of the Ediacaran Araras platform (Western Brazil) from the sedimentary and trace metals record. *Precambrian Research*, **241**:185-202. <https://doi.org/10.1016/j.precamres.2013.11.004>
- Santos J.O.S., Rizzotto G.J., Potterd P.E., McNaughton N.J., Matos R.S., Hartmann L.A., Chemale Jr. F., Quadros M.E.S. 2008. Age and autochthonous evolution of the Sunsás Orogen in West Amazon Craton based on mapping and U-Pb geochronology. *Precambrian Research*, **165**(3-4):120-152.
- Santos R.F., Nogueira A.C.R., Romero G.R., Soares J.L., Bandeira Júnior J. 2021. Life in the aftermath of Marinoan glaciation: The giant stromatolite evolution in the Puga cap carbonate, southern Amazon Craton, Brazil. *Precambrian Research*, **354**:106059. <https://doi.org/10.1016/j.precamres.2020.106059>
- Shields G.A. 2005. Neoproterozoic cap carbonates: a critical appraisal of existing models and the plume world hypothesis. *Terra Nova*, **17**(4):299-310. <https://doi.org/10.1111/j.1365-3121.2005.00638.x>
- Shields G.A. 2007. A normalised seawater strontium isotope curve: possible implications for Neoproterozoic-Cambrian weathering rates and the further oxygenation of the Earth. *eEarth*, **2**(2):35-42. <https://doi.org/10.5194/ee-2-35-2007>

- Sial A.N., Gaucher C., Misi A., Boggiani P.C., Alvarenga C.J.S., Ferreira V.P., Pimentel M.M., Pedreira J.A., Warren L.V., Fernández-Ramírez R., Geraldés M., Pereira N.S., Chiglino L., Cezario W.S. 2016. Correlations of some Neoproterozoic carbonate-dominated successions in South America based on high-resolution chemostratigraphy. *Brazilian Journal of Geology*, **46**(3):439-488. <https://doi.org/10.1590/2317-4889201620160079>
- Sial A.N., Gaucher C., Silva F.M.A., Ferreira V.P., Pimentel M.M., Lacerda L.D., Silva F.E.V., Cezario W. 2010. C-, Sr-isotope and Hg chemostratigraphy of Neoproterozoic cap carbonates of the Sergipano Belt, Northeastern Brazil. *Precambrian Research*, **182**(4):351-372. <https://doi.org/10.1016/j.precamres.2010.05.008>
- Soares J.L. 2012. *Paleoambiente e isótopos de C e O da capa carbonática de Tangará da Serra (MT), margem sul do cráton amazônico*. PhD Thesis. Instituto de Geociências, Universidade Federal do Pará, Belém, 152 p.
- Soares J.L., Nogueira A.C.R. 2008. Depósitos carbonáticos de Tangará da Serra (MT): uma nova ocorrência de capa carbonática neoproterozóica no sul do Cráton Amazônico. *Revista Brasileira de Geociências*, **38**(4):715-729.
- Soares J.L., Nogueira A.C.R., Santos R.F., Sansjofre P., Ader M., Truckenbrodt W., 2020. Microfacies, diagenesis and hydrocarbon potential of the Neoproterozoic cap carbonate of the southern Amazon Craton. *Sedimentary Geology*, **406**:105720. <https://doi.org/10.1016/j.sedgeo.2020.105720>
- Tucker M.E. 1992. *Sedimentary Petrology: an introduction to the origin of sedimentary rocks*. 2. ed. Durham: Blackwell Scientific Publications, 260 p.
- Van de Fliert T., Griffiths A.M., Lambelet M., Little S.H., Stichel T., Wilson D.J. 2016. Neodymium in the oceans: a global database, a regional comparison and implications for palaeoceanographic research. *Philosophical Transactions of the Royal Society A*, **374**(2081):20150293. <https://doi.org/10.1098/rsta.2015.0293>
- Verdel C., Phelps B., Welsh K. 2018. Rare earth element and  $^{87}\text{Sr}/^{86}\text{Sr}$  step-leaching geochemistry of central Australian Neoproterozoic carbonate. *Precambrian Research*, **310**:229-242. <https://doi.org/10.1016/j.precamres.2018.02.014>
- Wei G.Y., Hood A.V.S., Chen X., Li D., Wei W., Wen B., Gong Z., Yang T., Zhang Z.F., Ling H.F. 2019. Ca and Sr isotope constraints on the formation of the Marinoan cap dolostones. *Earth and Planetary Science Letters*, **511**:202-212. <https://doi.org/10.1016/j.epsl.2019.01.024>
- Wright D. 1999. The role of sulfate-reducing bacteria and cyanobacteria in dolomite formation in distal ephemeral lakes of the Coorong region South Australia. *Sedimentary Geology*, **126**(1-4):147-157. [https://doi.org/10.1016/S0037-0738\(99\)00037-8](https://doi.org/10.1016/S0037-0738(99)00037-8)
- Yang J., Jansen M.F., Macdonald F.A., About D.S. 2017. Persistence of a freshwater surface ocean after a snowball Earth. *The Geological Society of America*, **45**(7):615-618. <https://doi.org/10.1130/g38920.1>